Gold Nanoparticles Linked by Pyrrole- and Thiophene-Based Thiols. Electrochemical, Optical, and Conductive Properties

G. Zotti* and B. Vercelli

Istituto CNR per l' Energetica e le Interfasi, c.o Stati Uniti 4, 35127 Padova, Italy

A. Berlin*

Istituto CNR di Scienze e Tecnologie Molecolari, via C. Golgi 19, 20133 Milano, Italy

Received June 26, 2007. Revised Manuscript Received October 8, 2007

A series of new alkyl-substituted pyrrole, bithiophene, and terthiophene thiols, terthiophene and sexithiophene dithiols, and polythiophene polythiol have been synthesized. The compounds form self-assembled monolayers on gold with high surface coverages generally in the range (2–4) $\times$ 10^{-10} mol cm^{-2} as indicated by cyclic voltammetry and UV–vis spectroscopy. The thiols were reacted with 5 nm gold nanoparticles in toluene to form monodisperse, stable, and soluble thiol-capped gold clusters with the same gold core diameter, which were oxidatively coupled electrochemically (in solution or as films) and chemically (with iodine) to polymeric gold clusters. The dithiols (including ethanedithiol) and the polythiol formed analogous polymeric structures via layer-by-layer alternation with gold nanoparticles on gold-modified ITO and glass surfaces. The new materials were investigated by cyclic voltammetry, UV–vis and FTIR spectroscopy, and conductivity. The capped gold clusters display conductivities in the range 10^{-7}–10^{-2} S cm^{-1} and give solvoconductive responses fast and stable, which parallel the degree of swelling measured by QCM. The conductivities of the polymeric clusters are in the range 2 $\times$ 10^{-2}−10^{-1} S cm^{-1}. Comparison with the literature indicates 10^{-1} S cm^{-1} as a practical limit to the conductivity in such systems.

1. Introduction

Hybrid systems consisting of metal nanoparticles and organic compounds became an interesting research topic in recent years. The integration of metal nanoparticles into polymer matrixes attracts substantial research efforts directed to the development of hybrid materials for new catalytic, electronic, and optoelectronic applications.

In particular, hybrid materials containing metal nanoparticles and π-conjugated polymers (CPs)[1] have unique properties, and application of these materials in optoelectronic devices (such as solar cells, light-emitting diodes, electronic memories, etc.) is being explored intensively.[2] This combination is of high interest because of strong electronic interactions between the nanoparticles and the polymer matrixes. The conductivity of the hybrid systems is improved in the presence of metal nanoparticles embedded into the polymers. Thus, the electroswitchable conductivity of the nanoparticles/polymer system may be also applied to control the sensing properties of the hybrid system.

Among metal nanoparticles, gold nanoparticles (AuNPs) are particularly investigated,[3] and thiols are the linker moieties mostly used for them. Using α,ω-dithiols as spacer units between AuNPs, layer-by-layer (LBL) films attached to a solid substrate have been prepared.[4] Such materials show conductivities that mimic the behavior of semiconductors and that depend markedly on the length of the dithiol used to link the AuNPs together. Recently, a self-assembled polymeric monolayer, chemisorbed onto a gold surface via multiple thiol or disulfide groups grafted on the polymer backbone, has been reported.[5] As compared to organothiol SAMs, this self-assembled polymeric monolayer shows improved stability because of cooperative binding via multiple thiol–gold or disulfide–gold bonds.

Considering the combination of CPs and AuNPs, polyaniline (emeraldine polycation) has been multilayered with AuNPs,[6] and close-packed planar arrays of gold nanoclusters were covalently linked to each other by the rigid, double-ended organic molecules aryl α,ω-dithiols.[7] Polypyrrole, an excellent material to be used as a substrate or matrix for deposition of metal nanoparticles, has been used as template

* To whom correspondence should be addressed: tel (+39)49-8295868; fax (+39)49-8295853; e-mail g.zotti@ieni.cnr.it.

(1) Gangopadhyay, R.; De, A. *Chem. Mater.* **2000**, *12*, 608.
(2) (a) See e.g.: Huynh, W. U.; Dittmer, J. J.; Alivisatos, A. P. *Science* **2002**, *295*, 2425. (b) Dabbousi, B. O.; Bawendi, M. G.; Onitsuka, O.; Rubner, M. F. *Appl. Phys. Lett.* **1995**, *66*, 1316. (c) Tseng, R. J.; Huang, J.; Ouyang, J.; Kaner, R. B.; Yang, Y. *Nano Lett.* **2005**, *5*, 1077.
(3) Daniel, M. C.; Astruc, D. *Chem. Rev.* **2004**, *104*, 293.
(4) Brust, M.; Bethell, D.; Kiely, C.; Schiffrin, D. J. *Langmuir* **1998**, *14*, 5425.
(5) (a) Johnson, P. A.; Levicky, R. *Langmuir* **2003**, *19*, 10288. (b) Johnson, P. A.; Levicky, R. *Langmuir* **2004**, *20*, 9621.
(6) (a) Tian, S.; Liu, J.; Zhu, T.; Knoll, W. *Chem. Mater.* **2004**, *16*, 4103. (b) Granot, E.; Katz, E.; Basnar, B.; Willner, I. *Chem. Mater.* **2005**, *17*, 4600.
(7) Andres, R. P.; Bielefeld, J. D.; Henderson, J. I.; Janes, D. B.; Kolagunta, V. R.; Kubiak, C. P.; Mahoney, W. J.; Osifchin, R. G. *Science* **1996**, *273*, 1690.

10.1021/cm071701z CCC: $40.75
Published on Web 12/28/2007

support of AuNPs[8] and as nanotubules coated with AuNPs[9] but not in multilayers. AuNPs, capped by pyrrole decylthiol,[10,11] have been electropolymerized, and similarly 2-mercapto-3-octylthiophene has been used to cap AuNPs, thereby promoting their polymerization with 3-octylthiophene.[12] AuNPs quench very efficiently the fluorescence of polyfluorenes,[13] suggesting that the combination of conjugated polymers with these nanomaterials can potentially lead to improved sensitivity in optical biosensors. Finally, in a recent work[14] the electrodeposition and characterization of conducting thin films of AuNPs bridged with some phosphine-terminated oligothiophene linkers were reported. Their electrochemical oxidation results in the deposition of thin films consisting of nanoparticles linked by oligothiophene moieties.

We have undertaken a systematic approach to the synthesis of AuNPs-CPs materials in which the gold particles are connected by either CP bridges (Scheme 1a) or pendant from CP chains (Scheme 1b). The different patterns are characterized by different pathways for conduction, namely the direct bridge (along the gold–gold direction) and the sideway bridge (tangent to the gold particle).

The components of the projected structures have been selected on the basis of several stringent criteria. Concerning gold, the nanoparticles have been functionalized via the place-exchange method, by which the gold size is kept unchanged and is the same for all the used linkers.

For the linkers, first we have chosen pyrrole, bithiophene, and terthiophene thiols, terthiophene and sexithiophene dithiols, and polythiophene polythiol (see Chart 1) all with alkyl substitution. Capping of gold nanoparticles with oligothiophene thiols is not generally possible since aggregation is soon established by π-interactions between the oligothiophene backbones and the surfaces of AuNPs.[15] We have anyway shown that ring alkyl substitution overcomes this problem through steric hindrance of π-interactions.[15]

Second, pyrrole PY and dithiophene CPDT (Chart 1) have been selected to form structures of the bridge type vs the pendant type expected from the terthiophenes T3. The choice of terthiophenethiol instead of lower or higher oligothiophene thiols has been dictated by the requirements of high reactivity without degradation during oxidative coupling.

Third, in the case of thiophenes bearing the sulfur functionalization directly at the α-position of the thiophene ring, acetylthio-derivative or disulfides were preferred to the corresponding thiols since the direct connection of the thiol functionality to the conjugated chain makes the compound particularly unstable toward aerial disulfide formation. For the same reason the bifunctional and polyfunctional compounds, which could have produced polymers, were prepared as the acetylthio derivatives. In addition, after it has been shown that also acetylthio-capped molecules may form gold–sulfide links,[16] we have used also this moiety as capping agent.

Scheme 1

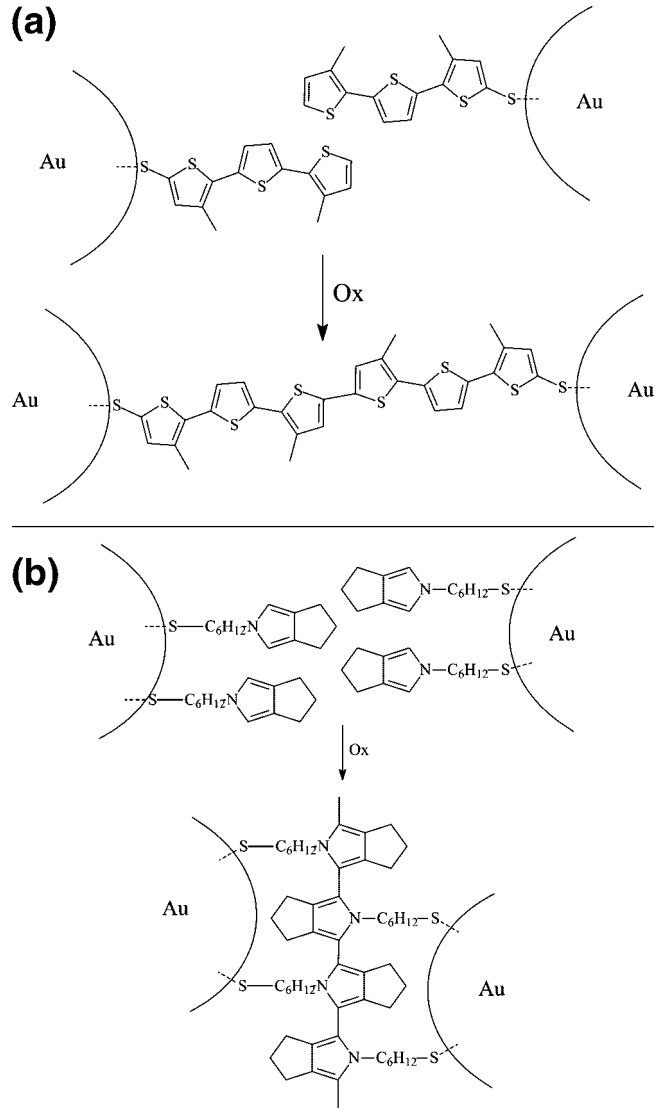

In this paper we report the synthesis of new alkyl-substituted pyrrole, bithiophene, and terthiophene thiols, the corresponding formation and characterization of SA monolayers on gold surfaces, the synthesis and characterization of AuNPs capped by the pyrrole- and thiophene-based thiols, the properties of the capped nanoparticles as films on electrodes, and their electrochemical and chemical oxidative polymerization to connected structures of the bridge or pendant type.

In order to compare the properties of the polymeric structures above with those obtained directly from α,ω-dithiols, the second section of the work reports the LBL connection of AuNPs with sexithiophene disulfides and, in

(8) (a) Marinakos, S. M.; Brousseau, L. C.; Jones, A.; Feldheim, D. L. *Chem. Mater.* **1998**, *10*, 1214. (b) Marinakos, S. M.; Novak, J. P.; Brousseau, L. C.; House, A. B.; Edeki, E. M.; Feldhaus, J. C.; Feldheim, D. L. *J. Am. Chem. Soc.* **1999**, *121*, 8518.
(9) He, Y.; Yuan, J.; Shi, G. *J. Mater. Chem.* **2005**, *15*, 859.
(10) Hata, K.; Fujihara, H. *Chem. Commun.* **2002**, 2714.
(11) Ito, M.; Tsukatani, T.; Fujihara, H. *J. Mater. Chem.* **2005**, *15*, 960.
(12) Peng, Z.; Wang, E.; Dong, S. *Electrochem. Commun.* **2002**, 210.
(13) (a) Fan, C.; Wang, S.; Hong, J. W.; Bazan, G. C.; Plaxco, K. W.; Heeger, A. J. *Proc. Natl. Acad. Sci. U.S.A.* **2003**, *100*, 6297. (b) Kim, K.; Sohn, B. H.; Jin, J. *J. Nanosci. Nanotechnol.* **2005**, *5*, 1898.
(14) Sih, B. C.; Teichert, A.; Wolf, M. O. *Chem. Mater.* **2004**, *16*, 2712.
(15) Zotti, G.; Vercelli, B.; Battagliarin, M.; Berlin, A.; Hernández, V.; López Navarrete, J. T. *J. Phys. Chem. C* **2007**, *111*, 5886.
(16) Lau, K. H. A.; Huang, C.; Yakovlev, N.; Chen, Z. K.; O'Shea, S. J. *Langmuir* **2006**, *22*, 2968.

Chart 1

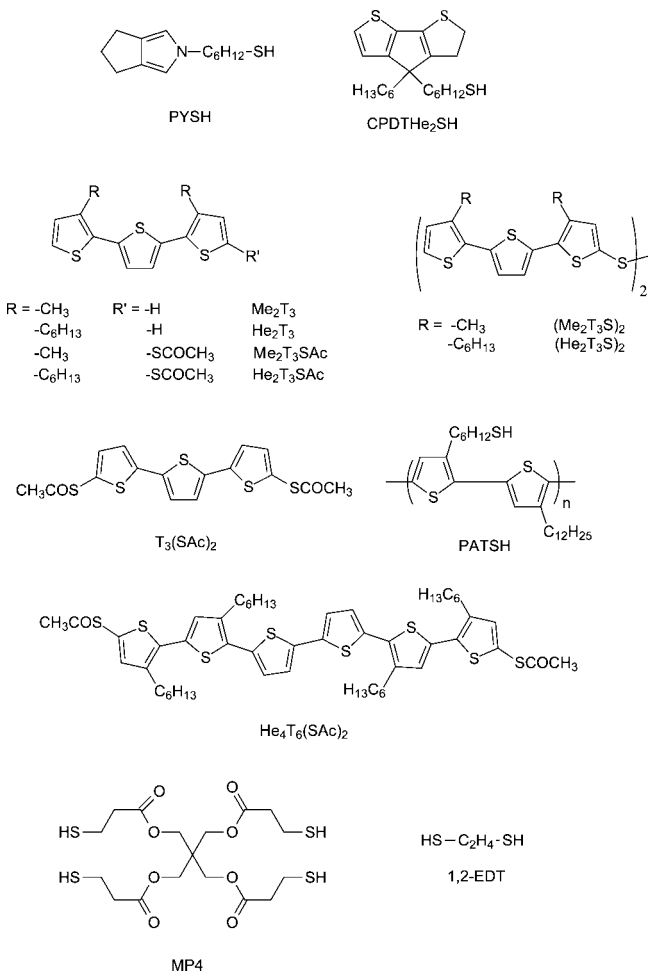

order to push the conductivity to higher levels, with shorter dithiols such as the conjugated T3-dithiol and the nonconjugated ethanedithiol. Finally, after a thiol-functionalized polyalkylthiophene, i.e., a regioregular alternate copolymer of 3-mercaptohexyl- and 3-dodecyl-substituted thiophene, has been prepared and used for microcontact printing,[17] we have prepared the analogous random-functionalized regioregular copolymer PATSH (Chart 1) and used it in the LBL formation of CP-connected AuNPs layers.

For all the produced structures a detailed conductivity and solvoconductivity analysis has been performed, and the results have been discussed and compared with those given in the literature.

2. Experimental Section

2.1. Chemicals and Reagents. All reactions of air- and water-sensitive materials were performed under nitrogen. Air- and water-sensitive solutions were transferred with double-ended needles. The solvents used in the reactions (Fluka) were absolute and stored over molecular sieves. Acetonitrile was reagent grade (Uvasol, Merck) with a water content <0.01%. The supporting electrolyte tetrabutylammonium perchlorate (Bu_4NClO_4), 3-mercaptopropyltrimethoxysilane (MTS), 1,2-ethanedithiol (EDT), and all other chemicals were reagent grade and used as received.

Toluene solutions of gold nanoparticles (AuNPs) stabilized by 0.05 M tetraoctylammonium bromide (TOABr) were prepared in 10^{-2} M gold concentration according to Brust and Schiffrin.[18] On the basis of TEM analysis, the average particle size of the Au clusters is 5 ± 1 nm (ca. 3600 gold atoms per cluster). AuNPs solutions for self-assembled layers were routinely 10^{-3} M gold concentration.

The compounds 2,4,5,6-tetrahydrocyclopenta[*c*]pyrrole (PY),[19] 6-(5,6-dihydro-4*H*-cyclopenta[*c*]pyrrol-2-yl)-hexane-1-thiol (PY-SH),[19] 3,3″-dimethyl-2,2′:5′,2″-terthiophene (Me_2T_3),[20] 3,3″-dihexyl-2,2′:5′,2″-terthiophene (He_2T_3),[21] 4-(6-bromohexyl)-4-hexyl-4*H*-cyclopenta[2,1-*b*:3,4-*b*′]dithiophene,[22] thioacetic acid *S*-(5″-acetylsulfanyl-2,2′:5′,2″-terthiophen-5-yl) ester [($T_3(SAc)_2$],[23] 5,5‴″-dibromo-3,4′,3‴,3‴″-tetrahexyl-2,2′:5′,2″:5″,2‴:5‴,2‴″:5‴″,2‴″-sexythiophene ($He_4T_6Br_2$),[24] 2-bromo-3-(6-bromohexyl)thiophene,[17] and 2-bromo-3-dodecylthiophene[25] were prepared as described in the literature.

Poly[3-(6-mercaptoheptyl)thiophene-*co*-3-dodecylthiophene] (PAT-SH) has been prepared from poly[3-(6-bromohexyl)thiophene-*co*-3-dodecylthiophene] following the same procedure described in the literature for the alternate copolymer.[17]

Regioregular head-to-tail coupled poly(3-octylthiophene) (P3OT), with degree of polymerization DP = ca. 120), has been produced chemically according to McCullough.[26]

^{1}H and ^{13}C NMR spectra were recorded on a Bruker FT 300 (300 MHz for ^{1}H); chemical shifts value are given in parts per million.

GPC measurements are referred to polystyrene as standard and were performed on a Waters Alliance 2000, equipped with a Millenium software, using CH_2Cl_2 as eluent.

Thioacetic Acid S-*(3,3″-Dimethyl-2,2′:5′,2″-terthiophen-5-yl) Ester (Me_2T_3SAc).* BuLi (1.6 M in hexane, 0.76 mL, 1.22 mmol) was added dropwise to a solution of Me_2T_3 (337 mg, 1.22 mmol) in THF (20 mL) at −78 °C. After 2 h of stirring, sublimated sulfur (41 mg, 1.28 mmol) was added, and the reaction mixture was stirred for 2 h at the same temperature and for 1 h at −20 °C. Acetyl chloride (96 mg, 1.22 mmol) was added dropwise, and the reaction mixture was stirred for 30 min at the same temperature and overnight at RT. The solvent was evaporated under reduced pressure. Flash chromatography of the residue (silica gel, petrol ether/CH_2Cl_2 8:2) afforded the title compound (277 mg, 65% yield). Anal. Calcd for $C_{16}H_{14}OS_4$: C, 54.82; H, 4.03%. Found: C, 54.67; H, 3.99%. ^{1}H NMR ($CDCl_3$): δ 2.39 (s, 3H), 2.42 (s, 6H), 6.89 (d, 1H), 6.94 (s, 1H), 7.09 (m, 2H), 7.16 (d, 1H). MS, *m/e* 350 ($M^{\bullet+}$).

Bis(3,3″-dimethyl-2,2′:5′,2″-terthiophen-5-yl) Disulfide ($Me_2T_3S)_2$]. A 25% aqueous solution of NH_4OH (1 mL) was added dropwise to a stirred solution of Me_2T_3SAc (137 mg, 0.39 mmol) in THF (10 mL). The reaction mixture was stirred for 3 h, neutralized with 1 M HCl, and extracted with ether. The organic phase was washed with water, dried (Na_2SO_4), and then evaporated

(17) Zhai, L.; Laird, D. W.; McCullough, R. D. *Langmuir* **2003**, *19*, 6492.
(18) Brust, M.; Bethell, D.; Schiffrin, D. J.; Kiely, C. *Adv. Mater.* **1995**, *7*, 795.
(19) Zotti, G.; Zecchin, S.; Schiavon, G.; Vercelli, B.; Berlin, A.; Grimoldi, S. *Macromol. Chem. Phys.* **2004**, *205*, 2026.
(20) Phan, C. V.; Burkhardt, A.; Shabana, R.; Cunninghan, D. D.; Mark, H. B.; Zimmer, H. *Phosphorus, Sulfur Silicon Relat. Elem.* **1989**, *46*, 153.
(21) Jones, C. L.; Higging, S. J. *J. Mater. Chem.* **1999**, *9*, 865.
(22) Zotti, G.; Zecchin, S.; Schiavon, G.; Berlin, A. *Macromolecules* **2001**, *34*, 3889.
(23) Taniguchi, S; Minamoto, M.; Matsushita, M. M.; Sugawara, T.; Kawada, Y.; Bethell, D. *J. Mater. Chem.* **2006**, *16*, 3459.
(24) Chen, C. H.; Liu, K. Y.; Sudhakar, S.; Lim, T. S.; Fann, W.; Hsu, C. P.; Luh, T. Y. *J. Phys. Chem. B* **2005**, *109*, 17887.
(25) Buvat, P.; Horquebie, P. *Macromolecules* **1997**, *30*, 2685.
(26) McCullough, R. D.; Lowe, R. D.; Jayaraman, M.; Anderson, D. L. *J. Org. Chem.* **1993**, *58*, 904.

to dryness. Flash chromatography of the residue (silica gel, petrol ether/CH_2Cl_2 8:3) gave the title compound as an orange solid (90 mg, 75% yield). Anal. Calcd for $C_{28}H_{22}S_8$: C, 54.69; H, 3.61%. Found: C, 54.56; H, 3.52%. ^{1}H NMR ($CDCl_3$): δ 2.38 (s, 3H), 2.41 (s, 6H), 6.89 (d, 1H), 7.00 (s, 1H), 7.09 (d, 1H), 7.12 (d, 1H), 7.15 (d, 1H). MS, *m/e* 614 ($M^{\bullet+}$).

Thioacetic Acid S-*(3,3″-Dihexyl-2,2′:5′,2″-terthiophen-5-yl) Ester (He_2T_3SAc).* This compound was prepared following the same procedure described above for the preparation of Me_2T_3SAc starting from He_2T_3. The title compound was obtained by flash chromatography of the residue (silica gel, petrol ether/CH_2Cl_2 9:1) (63% yield). Anal. Calcd for $C_{26}H_{34}OS_4$: C, 63.63; H, 6.98%. Found: C, 63.56; H, 6.91%. ^{1}H NMR ($CDCl_3$): δ 0.87 (t, 6H), 1.32 (m, 12H), 1.62 (m, 4H), 2.41 (s, 3H), 2.75 (m, 4H), 6.93 (d, 1H), 6.97 (s, 1H), 7.07 (m, 2H), 7.17 (d, 1H). ^{13}C NMR ($CDCl_3$): δ 14.05, 22.59, 29.21, 29.32, 29.69, 30.49, 30.68, 31.62, 31.67, 122.75, 123.94, 16.09, 126.67, 130.09, 134.82, 136.92, 138.37, 139.95, 140.23, 194.17. MS, *m/e* 490 ($M^{\bullet+}$).

Bis(3,3″-dihexyl-2,2′:5′,2″-terthiophen-5-yl) Disulfide [($He_2T_3S)_2$]. This compound was prepared following the same procedure described above for the preparation of $(Me_2T_3S)_2$ starting from He_2T_3SAc. The title compound was obtained by flash chromatography of the residue (silica gel, petrol ether/CH_2Cl_2 8:2) (70% yield). Anal. Calcd for $C_{48}H_{62}S_8$: C, 64.38; H, 6.98%. Found: C, 64.27; H, 6.95%. ^{1}H NMR ($CDCl_3$): δ 0.87 (t, 6H), 1.32 (m, 12H), 1.65 (m, 4H), 2.41 (s, 3H), 2.77 (m, 4H), 6.93 (d, 1H), 6.97 (s, 1H), 7.05 (m, 2H), 7.17 (d, 1H). MS, *m/e* 895 ($M^{\bullet+}$).

Thioacetic Acid S-*[6-(4-Hexyl-4*H*-cyclopenta[2,1-*b*:3,4-*b′*]dithiophen-4-yl)hexyl] Ester ($He_2CPDTSAc$).* A mixture of 4-(6-bromohexyl)-4-hexyl-4*H*-cyclopenta[2,1-*b*:3,4-*b′*]dithiophene (185 mg, 0.43 mmol), potassium thioacetate (500 mg, 4.37 mmol), and THF (10 mL) was refluxed under stirring for 6 h and stirred overnight at RT. Water was added, and the resulting mixture was extracted with CH_2Cl_2. The organic phase was dried (Na_2SO_4) and then evaporated to dryness. Flash chromatography of the residue (silica gel, petrol ether) gave the title compound as an oil (171 mg, 95% yield). Anal. Calcd for $C_{23}H_{32}OS_3$: C, 65.57; H, 7.67%. Found: C, 65.51; H, 7.59%. ^{1}H NMR ($CDCl_3$): δ 0.81 (t, 3H), 0.92 (m, 4H), 1.12 (m, 10H), 1.45 (m, 2H) 1.83 (m, 4H), 2.29 (s, 3H), 2.79 (t, 2H), 6.92 (d, 2H), 7.14 (d, 2H). MS, *m/e* 420 ($M^{\bullet+}$).

*6-(4-Hexyl-4*H*-cyclopenta[2,1-*b*:3,4-*b′*]dithiophen-4-yl)hexane-1-thiol ($He_2CPDTSH$).* $LiAlH_4$ (1 M in THF, 0.79 mL, 0.79 mmol) was added dropwise to a stirred solution of $He_2CPDTSAc$ (165 mg, 0.39 mmol) in THF (20 mL), keeping the temperature at 0 °C. The reaction mixture was stirred for 30 min at RT, a few drops of AcOEt were added, and stirring was continued for a further 30 min. 3 M HCl (10 mL) was added, and the resulting mixture was extracted with $CHCl_3$. The organic phase was washed with water, dried (Na_2SO_4), and then evaporated to dryness. Flash chromatography of the residue (silica gel, petrol ether/CH_2Cl_2) gave the title compound as an oil (171 mg, 95% yield). Anal. Calcd for $C_{21}H_{29}S_3$: C, 66.79; H, 7.74%. Found: C, 66.65; H, 7.71%. ^{1}H NMR ($CDCl_3$): δ 0.81 (t, 3H), 0.92 (m, 4H), 1.12 (m, 10H), 1.25 (t, 1H), 1.46 (m, 2H) 1.83 (m, 4H), 2.43 (m, 2H), 6.91 (d, 2H), 7.13 (d, 2H). ^{13}C NMR ($CDCl_3$): δ 13.98, 22.56, 24.36, 24.46, 28.07, 29.38, 29.66, 31.59, 33.85, 37.67, 37.85, 53.22, 121.58, 124.49, 136.50, 157.91. MS, *m/e* 420 ($M^{\bullet+}$).

Thioacetic Acid S-*(5‴″-Acetylsulfanyl-3,4′,3‴″,3‴″-tetrahexyl-2,2′:5′,2″:5″,2‴:5‴,2‴″:5‴″,2‴″-sexythiophen-5-yl) Ester [$He_4T_6(SAc)_2$].* BuLi (1.6 M in hexane, 0.13 mL, 0.21 mmol) was added dropwise to a solution of $He_4T_6Br_2$ (100 mg, 0.10 mmol) in THF (10 mL) at −78 °C. After 1 h of stirring, sublimated sulfur (7 mg, 0.22 mmol) was added, and the reaction mixture was stirred for 3 h at the same temperature. Acetyl chloride (16 mg, 0.20 mmol) was added dropwise, and the reaction mixture was stirred for 1 h at the same temperature and overnight at RT. The solvent was evaporated under reduced pressure. Flash chromatography of the residue (silica gel, petrol ether/CH_2Cl_2 8:2) afforded the title compound (60 mg, 61% yield). Anal. Calcd for $C_{52}H_{66}O_2S_4$: C, 63.76; H, 6.79%. Found: C, 63.72; H, 6.75%. ^{1}H NMR ($CDCl_3$): δ 0.89 (m, 12H) 1.33 (m, 24H), 1.65 (m, 8H), 2.42 (s, 6H), 2.76 (m, 8H), 6.97 (s, 4H), 7.05 (d, 2H), 7.14 (d, 2H). FABMS, *m/z* 979 $(M + H)^+$.

Poly[3-(6-bromohexyl)thiophene-co-*3-dodecylthiophene].* BuLi (1.6 M in hexane, 4.0 mL, 6.40 mmol) was added dropwise to a stirred solution of diisopropylamine (787 mg, 7.78 mmol) in THF (20 mL) at −70 °C, and the solution was stirred for 1.5 h. A solution of 2-bromo-3-(6-bromohexyl)thiophene (1.06 g, 3.19 mmol) and of 2-bromo-3-dodecylthiophene (1.04 g, 3.19 mmol) in THF (2 mL) was added dropwise, and the resulting mixture was stirred for 2 h. $ZnCl_2$ beads (0.87 g, 6.40 mmol) were added in one portion, and the reaction was stirred until all $ZnCl_2$ was dissolved. The mixture was warmed to −5 °C, and $NiCl_2$(dppp) (18 mg, 0.03 mmol) was added. The reaction mixture was allowed to warm to RT and stirred overnight. Methanol (70 mL) was added, and the polymer precipitate was collected by filtration and washed with methanol, followed by hexane in a Soxhlet extractor. The polymer was dissolved by Soxhlet extraction with $CHCl_3$. The solvent was evaporated under reduced pressure to give the title 97% head-to-tail coupled copolymer (1.43 g, 45% yield) in a 1:1 monomer ratio. ^{1}H NMR ($CDCl_3$): δ 0.86 (t, 3H), 1.49–1.25 (m, 22H), 1.69 (m, 4H), 1.89 (t, 3H), 2.81 (m, 4H), 3.41 (t, 2H), 6.97 (s, 2H). M_n = 16 620, M_w/M_n = 1.93 by GPC.

2.2. Substrates and Multilayer Film Formation. Transparent gold-coated surfaces were prepared from glass sheets or indium tin oxide (ITO)/glass electrodes (20 Ω sq^{-1} from Merck-Balzers) by treatment with 3-mercaptopropyltrimethoxysilane (MTS),[27] which provides on both sides a surface bearing free thiol groups, and subsequently with 10^{-3} M toluene solution of AuNPs for 18 h, which deposits a monolayer of them on the thiol surface.

Gold electrodes were 1 × 4 cm^2 sheets. They were treated for 1 min with hot sulfochromic acid ($K_2Cr_2O_7$ in 96% H_2SO_4), then carefully washed with Milli-Q water, and dried.[28]

The buildup of multilayers on ITO/glass electrodes was performed according to the methodology introduced by Decher,[29,30] i.e., by dipping the electrodes alternatively into the solutions of the two components. Immersion times were 2 h. After each immersion step the substrate was carefully washed and dried in air. The layer buildup was monitored by UV–vis spectroscopy and cyclic voltammetry.

2.3. SAMs of Thiols on Gold. SAMs were produced by overnight immersion of gold electrodes in 10^{-3} M ethanol solutions of PYSH or He_2T_3SAc and Me_2T_3SAc, then careful rinsing with ethanol, and drying. In the case of $(He_2T_3S)_2$, $(Me_2T_3S)_2$, or $He_2CPDTSH$, a CH_2Cl_2–ethanol 1:1 mixture was used due to solubility reasons, followed by rinsing with CH_2Cl_2 and drying.

PATSH monolayers on gold were similarly produced in a 10^{-4} M (as thiophene subunits) solution of PATSH in chloroform (where the polymer is stable for weeks), then rinsing with chloroform, and drying.

(27) Goss, C. A.; Charych, D. H.; Majda, M. *Anal. Chem.* **1991**, *63*, 85.
(28) Kang, J.; Rowntree, P. A. *Langmuir* **2007**, *23*, 509.
(29) (a) Decher, G.; Hong, J. *Makromol. Chem., Macromol. Symp.* **1991**, *46*, 321. (b) Decher, G.; Hong, J. *Ber. Bunsenges. Phys. Chem.* **1991**, *95*, 1430. (c) Decher, G. *Science* **1997**, *277*, 1232.
(30) Lvov, Y.; Decher, G.; Mohwald, H. *Langmuir* **1993**, *9*, 481.

EDT layers on gold were formed according to the literature[31] using a 10^{-3} M solution of the dithiol in ethanol and an exposure time of 1 h.

SAMs of $He_4T_6(SAc)_2$ on gold were produced from a freshly prepared 10^{-4} M solution in CH_2Cl_2 + 10% acetone added with a few drops of ammonia (which converts acetylthiols to thiols) for 2 h, then rinsing with CH_2Cl_2, and drying. In the case of $T_3(SAc)_2$, SAMs were produced by overnight immersion in a 5×10^{-4} M solution in acetonitrile, then rinsing with acetonitrile, and drying.

2.4. Synthesis of Thiol-Capped AuNPs. In the case of PYSH, 20 μL of a 0.5 M solution of PYSH in chloroform (10 μmol) was added to a 10^{-2} M toluene solution of AuNPs (10 mL, 100 μmol), and the resulting solution was allowed to stay for 24 h at room temperature. The solvent was then evaporated, and the solid was carefully washed with acetonitrile and ethanol (50 mL each) to remove alkyl bromide and nonreacted thiol. Then the solid was redissolved in chloroform, the solvent evaporated, and the solid washed again with ethanol and acetonitrile to produce ca. 20 mg of product.

The same procedure was used with Me_2T_3SAc, He_2T_3SAc, $(He_2T_3S)_2$, and $He_2CPDTSH$ (5 mg each).

The nanoparticles are soluble in toluene and chloroform but insoluble in acetonitrile and ethanol.

2.5. Apparatus and Procedure. *Electrochemistry and Spectroscopy.* Experiments were performed at room temperature under nitrogen in three electrode cells. The counter electrode was platinum; unless stated differently, the reference electrode was a silver/0.1 M silver perchlorate in acetonitrile (0.34 V vs SCE). The voltammetric apparatus (AMEL, Italy) included a 551 potentiostat modulated by a 568 programmable function generator and coupled to a 731 digital integrator.

The working electrode for solution cyclic voltammetry (CV) was a platinum minidisc electrode (0.003 cm^2). For solid-state CV a 1 $\times$ 2 cm^2 ITO/glass sheet (ca. 20 ohm/square resistance) was used.

Electronic spectra were run on a Perkin-Elmer Lambda 15 spectrometer; FTIR spectra were taken on a Perkin-Elmer 2000 FTIR spectrometer. FTIR spectra of films were taken in reflection–absorption mode.

Conductivity. The apparatus and procedures used for conductivity experiments were previously described in detail.[32,33] The electrode was a microband array platinum electrode (5 μm bandwidth, 100 nm thick) with interband spacing of 5 μm. The deposit was thick enough to ensure minimum resistance, under which condition the conductivity σ is given by $\sigma = k/(R - R_0)$, where R is the measured resistance, R_0 the lead resistance, and k the cell constant. These electrodes were used also for solvoconductivity measurements.

Measurements of the sheet resistance of multilayers were performed on the float glass side of the substrate with the four-probe technique using a Kuliche-Soffa head (UK) with a Keithley 220 programmable current source and a Keithley 195A digital multimeter.

AFM and Profilometry. Atomic force microscopy (AFM) was performed in noncontact mode in air at room temperature using a DME DS 95-200 Dualscope STM equipped with noncontact mode silicon tips. Multilayer thicknesses were determined with an Alphastep IQ profilometer from KLA Tencor.

QCM Sensor. Quartz crystal microbalance (QCM) analysis was performed with a platinum-coated AT-cut quartz electrode (0.2 cm^2), resonating at 9 MHz, onto which the clusters were deposited.

Scheme 2

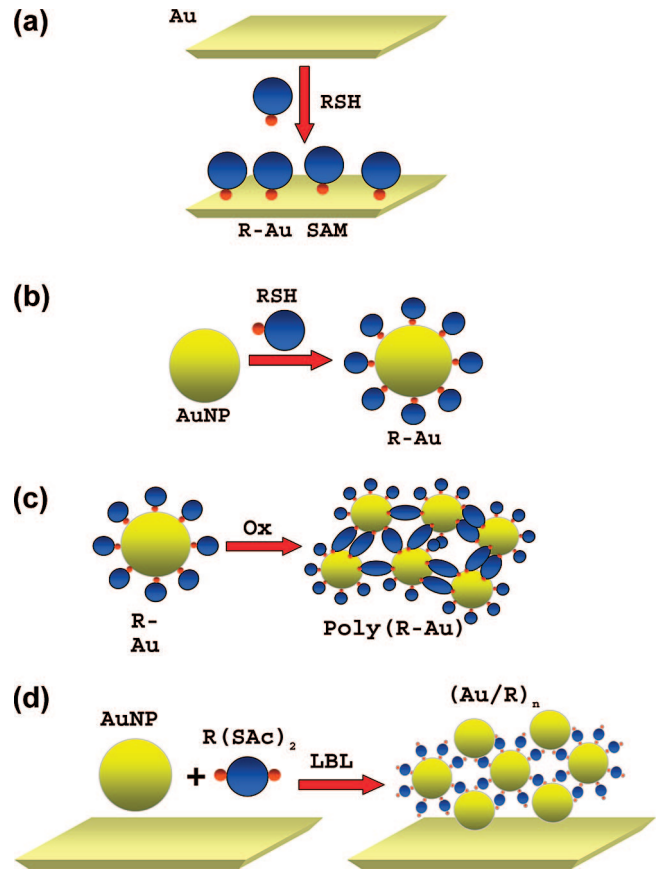

The oscillator circuit was homemade, and the frequency counter was a Hewlett-Packard model 5316B.

3. Results and Discussion

3.1. Thiol-Capped Gold Surfaces. SAMs were first produced on gold electrodes (and named R-Au SAM, see Scheme 2a) by immersion in a solution of the corresponding thiol RSH or disulfide $(RS)_2$ as detailed in the Experimental Section. This allowed to give a first estimation of the amount of ligand which could be assembled on a gold surface and its characteristics. SAMs were investigated by both reductive and oxidative CV. The electrochemical reduction–desorption of the monolayers was performed in 0.5 M KOH down to –1.2 V vs SCE,[34] whereas the electrochemical oxidation was performed in acetonitrile + 0.1 M Bu_4NClO_4 up to 0.9 V vs Ag/Ag^+. A single CV cycle at a scan rate of 0.1 V s^{-1} was generally used. SAMs were also produced on AuNPs-primed glass to evaluate their optical characteristics. The obtained electrochemical parameters are summarized in Table 1.

3.1.1. Pyrrole. Reduction–desorption CV of the PY–Au SAMs reveals the presence of two reduction peaks. Two peaks are accounted for by the polycrystalline nature of the gold surface, which presents different sites (crystal faces or step sites) of adsorption.[35] The stripping charge involved in

(31) Joo, S. W.; Han, S. W.; Kim, K. *Langmuir* **2000**, *16*, 5391.
(32) Schiavon, G.; Sitran, S.; Zotti, G. *Synth. Met.* **1989**, *32*, 209.
(33) Aubert, P. H.; Groenendaal, L.; Louwet, F.; Lutsen, L.; Vanderzande, D.; Zotti, G. *Synth. Met.* **2002**, *126*, 193.
(34) Yang, D. F.; Wilde, C. P.; Morin, M. *Langmuir* **1996**, *12*, 6570.
(35) Walkzak, M. M.; Alves, C. A.; Lamp, B. D.; Porter, M. D. *J. Electroanal. Chem.* **1995**, *396*, 103.

Table 1. Oxidation Peak Potentials (E^p) and Absorption Maxima (λ) of Linkers in Solution, Oxidation Peak Potentials (E^p_{ox}), Surface Charge Density (Q_{ox}), Reduction–Desorption Peak Potentials (E^p_{red}), Surface Charge Densities (Q_{red}), and Coverage (Γ) of Linkers as Monolayers on Gold

linker	E^p/V[a]	λ/nm[b]	E^p_{ox}/V	Q_{ox}/μC cm^{-2}	E^p_{red}/V[c]	Q_{red}/μC cm^{-2}	$\Gamma/10^{-10}$ mol cm^{-2}
PYSH	0.72	234[d]	0.42	100	−0.45; −0.96	40	4
$(He_2T_3S)_2$	0.65	357	0.70	30	−0.92	20	2
$(Me_2T_3S)_2$	0.65	359	0.70	60	−0.92	30	3
He_2CPDTSH	0.68	320	0.60	80	−1.00	40	4
$He_4T_6(SAc)_2$	0.55[e]	420	0.65[e]	80	−0.95	40	4
$T_3(SAc)_2$	0.73	375	0.79	95	−0.62; −0.92	60	6
PATSH	0.15; 0.55	450	0.57[e]	50			17[f]
EDT					−0.96	180	

[a] 10^{-3} M in acetonitrile at 0.1 V s^{-1}. [b] In chloroform. [c] vs SCE. [d] In acetonitrile. [e] E^0. [f] In repeat units.

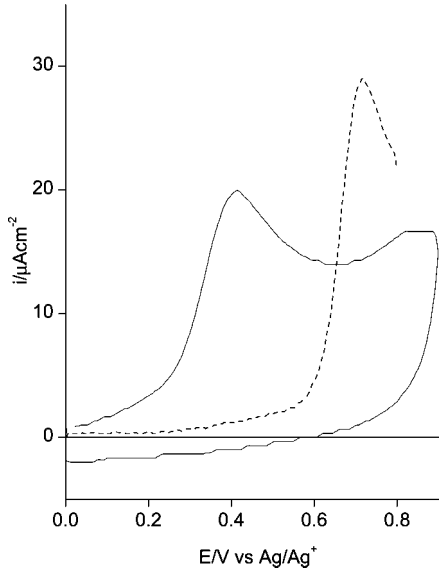

Figure 1. Oxidative CV of PYSH monolayer on gold in acetonitrile + 0.1 M Bu_4ClO_4. Scan rate: 0.1 V s^{-1}. Dashed line: CV of PYSH in solution for comparison.

the overall one-electron reduction corresponds to a coverage of 4×10^{-10} mol cm^{-2}.

The monolayers are irreversibly oxidized (Figure 1), and from the oxidation charges involved in the CV cycle, assuming that the process is a two-electron one,[36] the coverage degree is ca. 5×10^{-10} mol cm^{-2}, in substantial agreement with the evaluation based on the cathodic charge. Both values agree with that given in the literature for analogous *N*-alkanethiol monolayers[3] and correspond to that of a dense ferrocene monolayer.[37]

Since the parent *N*-hexyl-cyclopenta[*c*]pyrrole (PY) shows an irreversible oxidation process at $E_p = 0.72$ V,[19] a strongly negative shift (−0.3 V) of the monolayer oxidative E_p from the value for the compound in solution is clearly apparent. This result may be attributed to a strong stabilization of the oxidized monolayer at densely covered sites by π-dimerization of initially formed radical cations.[38]

No polymer is produced by oxidative CV as evidenced by the subsequent absence of redox processes around −0.1 V,[19] which indicates preferred degradation. This outcome was previously obtained also with non-3,4-capped thiol–pyrrole monolayers[39] which localizes the degradation at the 2,5-coupling sites of the pyrrole ring.

In any case potentiostatic oxidation of PY ((2–4) $\times 10^{-3}$ M) at 0.8 V on the PY–Au monolayer with the passage of 5 mC cm^{-2} (which does not form polymer layers by itself) produces surface coupling with formation of a poly(PY) layer, as shown by the obtained redox response at $E^0 =$ ca. −0.1 V storing a reversible charge of ca. 60 μC cm^{-2} (measured at 0.8 V). This result suggests that coupling of PY ligands is possible in the used media on condition that a correct (*anti*) alignment of the pyrrole rings is allowed. This condition is not fulfilled in the monolayer where the rings are in the *sin* disposition but is possible between pyrrole rings on the surface and others coming from the solution. Therefore cross-coupling of pyrrole-capped nanoparticles is feasible, as will be shown in following sections.

3.1.2. Terthiophene. For this investigation we have used both disulfides and acetylthio derivatives without difference in the obtained structures.

The electrochemical reduction–desorption of the He_2T_3–Au and Me_2T_3–Au SAMs has shown in this case only one reduction peak in which the passed charge corresponds to a coverage of 2×10^{-10} and 3×10^{-10} mol cm^{-2}, respectively.

The SAMs are irreversibly oxidized with a charge which, given a two-electron irreversible oxidation, corresponds to the same evaluated from reduction. The oxidation potential is in this case comparable to that of other terthiophenes (see Table 1) which may be attributed to reciprocal steric repulsion in the layers hindering π-stabilization of radical cation intermediates. In the case of He_2T_3–Au oxidation is a broad ill-defined process, difficult compared with that of the methyl analogue, which is attributed to a slower electron transfer, displayed also by the corresponding thiol-modified AuNPs (see below).

Me_2T_3–Au and He_2T_3–Au SAMs on AuNPs-primed glass show the band of the adsorbed terthiophene monolayer at 400 nm, i.e., with a strong red shift from the value of the free oligomer in solution (360 nm) caused by interaction of the π-system with the gold particles (see below). The absorbance values correspond to a coverage of (2–3) $\times 10^{-10}$ mol cm^{-2}, in perfect agreement with the electrochemical results.

3.1.3. Cyclopentadithiophene. In this case we report first the behavior of the thiol in solution since its oxidative

(36) Willicut, R. J.; McCarley, R. L. *J. Am. Chem. Soc.* **1993**, *116*, 10823.
(37) Gui, J. Y.; Stern, D. A.; Lu, F.; Hubbard, A. T. *J. Electroanal. Chem.* **1991**, *305*, 37.
(38) Miller, L. L.; Mann, K. R. *Acc. Chem. Res.* **1996**, *29*, 417 and references therein.
(39) (a) Collard, D. M.; Sayre, C. N. *J. Electroanal. Chem.* **1994**, *375*, 367. (b) Willicut, R. J.; McCarley, R. L. *Langmuir* **1995**, *11*, 296. (c) Wurm, D. B.; Brittain, S. T.; Kim, Y. T. *Langmuir* **1996**, *12*, 3756.

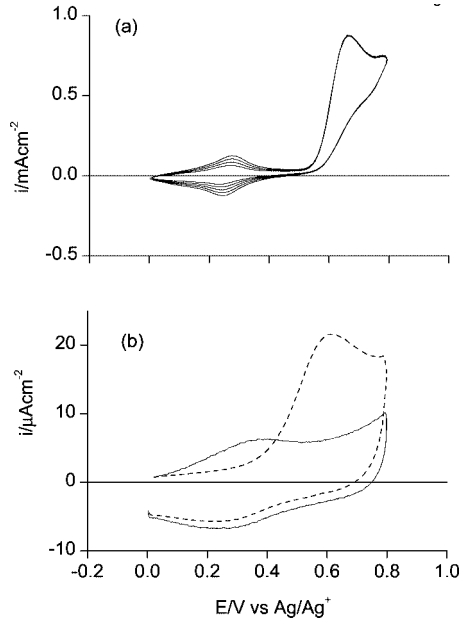

Figure 2. Oxidative CV of He_2CPDTSH (a) 10^{-3} M solution and (b) monolayer on gold in acetonitrile + 0.1 M Bu_4ClO_4. Scan rate: 0.1 V s^{-1}; (---) first and (—) following scans.

electrochemistry, differently from the pyrrole and the terthiophenes above, leads to polymeric products on the SA electrode.

The oxidation process of He_2CPDTSH dissolved in acetonitrile is shown at $E_p = 0.68$ V (Figure 2a). Oligomers produced by CV cycling on the electrode surface are evidenced in monomer-free electrolyte at $E^0 = 0.20$ V. As film deposited on ITO, the oligomer deposit displays a band at $\lambda_{max} = 545$ nm vs 320 nm for the monomer in solution. For comparison, the thiol-free analogue poly(He_2CPDT) film, with a FTIR-based degree of polymerization DP = 10, displays $E^0 = 0.07$ V and $\lambda_{max} = 590$ nm[40] so that a DP = 3–5 (6–10 thiophene rings) may be interpolated for our oligomeric system. The difference may be attributed to additional interactions between the oligomers via the thiol ends promoting their earlier precipitation.

Considering the He_2CPDT–Au SAMs, electrochemical reduction–desorption occurs in one reduction peak. The monolayers are irreversibly oxidized in a well-defined process (Figure 2b) with an oxidation charge once more twice the reduction stripping charge. The oxidation potential is less positive (by ca. 0.1 V) than for the solution value as expected from a moderate π-stabilization of oxidized intermediates. Subsequent CVs show the presence of a surface redox process at $E^0 = 0.30$ V, attributable to oligomers produced by cross-coupling. The whole behavior is similar to that previously observed on carboxyl-terminated CPDT compounds on ITO[41] so that the polymers are in fact oligomers and more probably sexithiophenes.[41]

These results indicate that in this case coupling occurs between units on the same surface and therefore that in CPDT-capped nanoparticles (see below) self-coupling may be in competition with cross-coupling of the nanoparticles.

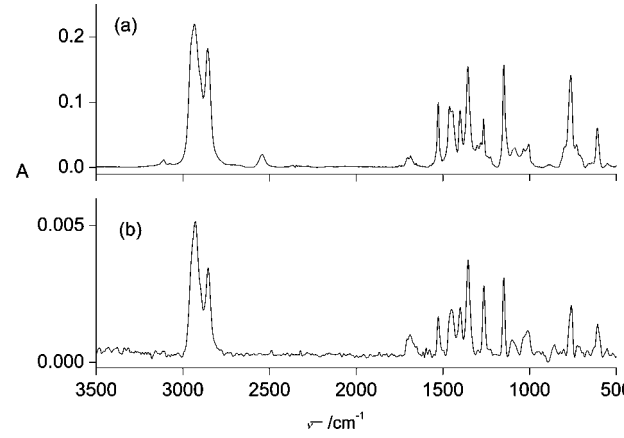

Figure 3. FTIR spectra of (a) PYSH and (b) PY–Au film on platinum.

3.2. Thiol-Capped AuNPs. AuNPs capping with a thiol RSH is illustrated in Scheme 2b where the produced nanoparticles are named R–Au.

R–Au nanoparticles are prepared via the place-exchange method,[42] i.e., through functionalization of TOABr-capped gold nanoparticles with RSH, as detailed in the Experimental Section. Since we have about 3600 gold atoms per cluster and a coverage of (2–4) × 10^{-10} mol cm^{-2} was measured in R–Au monolayers (see above), we estimated that 100–200 molecules are adsorbed on the surface. On this basis we have calculated the thiol molar amount required and used a 2-fold excess of it for the synthesis.

The presence of nonreacted AuNPs in the reaction batch is ruled by the absence of gold suspensions in subsequent solutions. In fact, ethanol washing of evaporated AuNPs deposits removes the alkyl bromide completely, causing gold aggregation to insoluble gold grains. On the contrary, excess ligand was in any case recovered in the washings.

3.2.1. Pyrrole-Capped AuNPs. The surface modification of electrodes with gold–polymer films has been performed in the past via the electrochemical oxidative polymerization of pyrrole-based nanoparticles,[10] but the resulting gold–polypyrrole composite material did not show electroactivity of the polypyrrole component, probably due to overoxidation at the free 3- and 4-positions of the pyrrole ring. For this reason we have capped gold nanoparticles with PYSH, namely *N*-pyrrolylhexanethiol, with cyclopropane capping of the 3,4-positions of pyrrole.

The UV–vis spectrum of the PY–Au nanoparticles in toluene solution exhibits the gold SP band at 520 nm, i.e., close to that for the starting AuNPs. This confirms that the size of the gold cluster has been kept essentially unchanged and that the pyrrole ring, separated by the alkyl chain, does not exert any influence on the gold cluster. The signals in the FTIR spectrum of the PY–Au nanoparticles (Figure 3b) correspond substantially to those of free PYSH (Figure 3a) but for the significant disappearance of the S–H stretching band at 2540 cm^{-1} supporting the occurred surface immobilization.

3.2.2. Oligothiophene-Capped AuNPs. The UV–vis spectrum of the He_2T_3–Au nanoparticle solution in toluene

(40) Zotti, G.; Schiavon, G.; Berlin, A.; Pagani, G. *Macromolecules* **1994**, *27*, 1938.
(41) Berlin, A.; Zotti, G.; Schiavon, G.; Zecchin, S. *J. Am. Chem. Soc.* **1998**, *120*, 13453.
(42) VanHerrikhuyzen, J.; Janssen, R. A. J.; Meijer, E. W.; Meskers, S. C. J.; Schenning, A. P. H. J. *J. Am. Chem. Soc.* **2006**, *128*, 686.

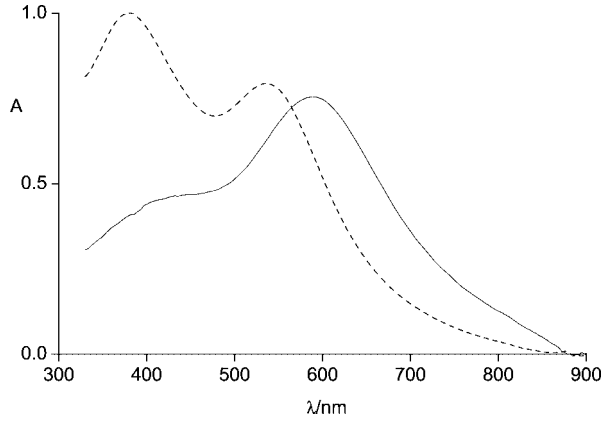

Figure 4. UV–vis spectra of He_2T_3–Au (---) in toluene solution and (—) as film on ITO.

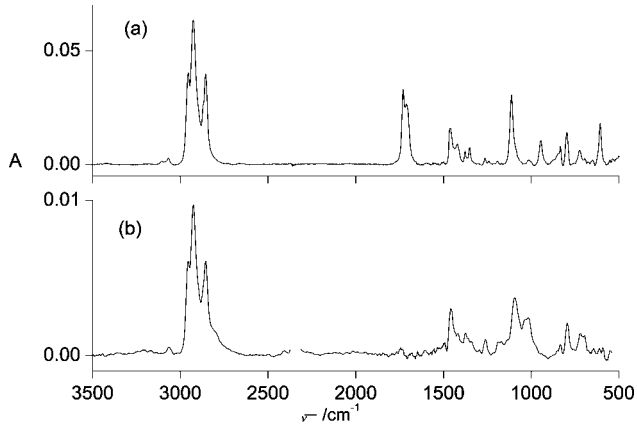

Figure 5. FTIR spectra of (a) He_2T_3SAc and (b) He_2T_3–Au film on platinum.

(Figure 4) exhibits the SP band at 535 nm, with a 10 nm red shift compared with the free AuNPs. This is attributable to coupling of the SP with the π-system of T_3, which is not operating in PY–Au due to the long alkyl spacer. For analogous reasons a band at 382 nm, signaling the presence of coordinated He_2T_3 moieties, is red-shifted strongly (by 25 nm) compared to the band (357 nm) of the $(He_2T_3S)_2$ molecule in the same solvent (see above). The spectra of the Me_2T_3–Au nanoparticles are the same of the He_2T_3 analogues.

The UV–vis spectrum of the He_2CPDT–Au nanoparticle solution in toluene exhibits the SP band at 525 nm, i.e., with no red shift compared with free AuNPs. In fact, in this case no significant coupling of the SP with the π-system of the bithiophene is operating due to the long alkyl spacer. A band at 317 nm, signaling the presence of coordinated He_2CPDT, is also shown.

Spectra of films cast on ITO (Figure 4) show the oligothiophene and gold maxima red-shifted to 400 and 590 nm (560 nm for He_2CPDT–Au), respectively.

The use of acetylthio ends in the ligand has allowed to show clearly the occurrence of the surface reaction. In fact, the signals in the FTIR spectrum of the He_2T_3–Au nanoparticles produced from He_2T_3SAc (Figure 5b) correspond substantially to those of free He_2T_3SAc (Figure 5a) but for the clear disappearance of the strong CO stretching band at 1720 cm^{-1}, in agreement with surface immobilization via sulfide bonds.

Table 2. Cluster and Poly(cluster)[a] Film Absorption Maximum (λ_c and λ_p) and Conductivity (σ_c and σ_p); Redox Oxidation Potentials (E^0_{ox}) of Poly(cluster) Films

cluster	λ_c/nm	λ_p/nm	σ_c/S cm^{-1}	σ_p/S cm^{-1}	E^0_{ox}/V
PY–Au	–, 560	290, 580	3×10^{-7}	5×10^{-2}	0.10
He_2T_3–Au	400, 590	440, 660	1×10^{-3}	1×10^{-1}	0.65
Me_2T_3–Au	400, 590	440, 660	2×10^{-4}	2×10^{-2}	0.55
He_2CPDT–Au	400, 560	560	1×10^{-2}		0.30
$(Au/PAT)_{10}$		450, 560		2×10^{-2}	0.46; 0.61
$(Au/He_4T_6)_5$		445, 610		5×10^{-2}	0.65
$(Au/T_3)_5$		440, 640		1×10^{-1}	
$(Au/EDT)_5$		750		2.5	

[a] From iodine coupling.

3.3. Coupling of Thiol-Capped AuNPs. Coupling of thiol-capped AuNPs R-Au to polymeric clusters poly(R-Au), illustrated in Scheme 2c, has been performed both electrochemically and chemically.

The electrochemical behavior of R–Au nanoparticles was studied by cyclic voltammetry in the solid state and in solution. For solid-state analysis R–Au films were cast from chloroform solution and subsequent CV analysis was performed in acetonitrile with added 0.1 M Bu_4NClO_4. Solution electrochemistry of R-Au was generally performed in CH_2Cl_2 or 1:1 $CH_2Cl_2/CHCl_3$ with added 0.1 M Bu_4NClO_4 and containing the R–Au nanoparticles in 10^{-2} M gold concentration.

Films of R-Au nanoparticles were also chemically coupled by iodine. After exposure to iodine vapor for 10 min, the samples are washed with acetone, which operates the complete loss of iodine, and then with chloroform and dried. The intensity of FTIR spectra indicates that no appreciable loss of material has occurred. The initial clusters have become insoluble, thus confirming the occurred polymerization.

In order to support the regular occurrence of coupling, we have applied the same treatment to films of α-methyl-capped terthiophene. The reaction has produced a dark red material which dissolves in warm chlorobenzene to yield the spectrum at 445 nm of the α,ω-dimethyl-capped sexithiophene.[43] This result, while confirming that the radical cation produced by iodine in terthiophenes couples to dimer, certifies that the residual free and/or dopant iodine is easily removed by washing with acetone. The coupling reaction works efficiently with all the terthiophene-, cyclopentadithiophene-, and pyrrole-based ligands here investigated, as suggested by the proximity of their oxidation potentials (see Table 1) and confirmed by the analytical results reported below for the individuals. Electrochemical and optical parameters of the produced polyclusters are summarized in Table 2.

3.3.1. Pyrrolethiol-Capped AuNPs. *Solid-State Electrochemical Coupling.* PY–Au films show an irreversible oxidation (Figure 6) at the same potential of the PY–Au SAM on the gold electrode. Upon repetitive cycling the CV develops a redox response at $E^0 = 0.10$ V (Figure 6) attributable to polypyrrole moieties formed by anodic coupling. This potential is higher than that of poly(PY) ($E^0 = -0.05$ V[19]) which is accounted for by a lower degree of polymerization,

(43) Zotti, G.; Schiavon, G.; Berlin, A.; Pagani, G. *Chem. Mater.* **1993**, *5*, 620.

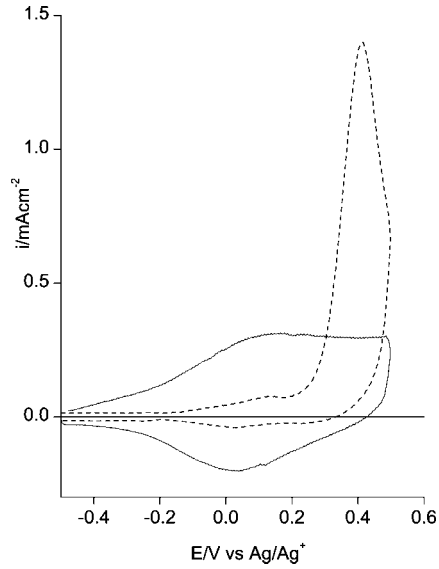

Figure 6. Cyclic voltammograms of PY–Au film in acetonitrile + 0.1 M Bu_4NClO_4 (---) first scan and (—) after potentiostatic oxidation at 0.5 V. Scan rate: 0.1 V s^{-1}.

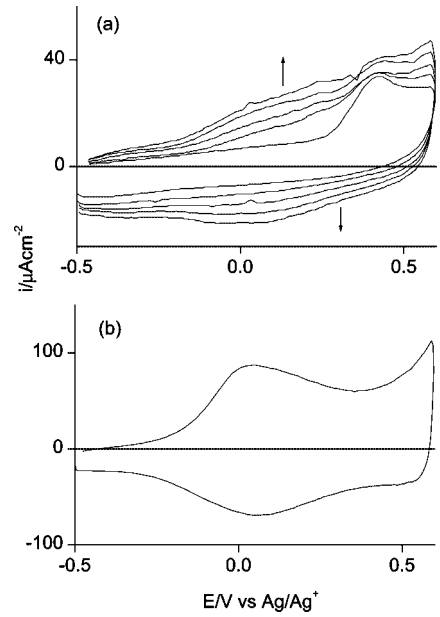

Figure 7. Cyclic voltammograms of (a) PY–Au solution in CH_2Cl_2 + 0.1 M Bu_4NClO_4 and (b) poly(PY–Au) film in acetonitrile + 0.1 M Bu_4NClO_4. Scan rate: 0.1 V s^{-1}.

expected from the limited contact area among gold nanoparticles. Interpolating between the potential values of the monomer and the polymer (DP = 13[19]), we may estimate a DP = ca. 4 for the oligomeric chains linking the gold particles. The resulting organometallic polymer layer is insoluble in chloroform, thus supporting the occurrence of cross-linking. The reversible charge is ca. 30% of the total irreversible oxidation charge which indicates that electrochemical cross-linking is highly efficient.

Solution Electrochemical Coupling. The cyclic voltammogram of PY–Au dissolved in CH_2Cl_2 shows the irreversible oxidation peak of the pyrrole moieties at $E_p = 0.40$ V. With repetitive scans, an increase in the CV response is observed at $E^0 = 0.1$ V as indication of the polymer growth (Figure 7a). The subsequent CV in monomer-free solution shows the cyclic voltammogram of poly(PY–Au) (Figure 7b) similar with that of poly(PY).

Deposition proceeds regularly with a high charge yield of ca. 35% (one reversible electron per three oxidation electrons) and with stored charges up to ca. 1 mC cm^{-2}, beyond which the CV is distorted (forward an backward peaks separate progressively), which may be attributed to the resistivity of the deposit (see below). The limiting thickness is lower than 1 μm, which precludes the possibility of in situ conductivity measurements on such deposits.

SP Band Bleaching. Anodic deposition of poly(PY–Au) produces a smooth film with maximum of the SP band at 550 nm (Figure 8a). The spectrum of the electrochemically deposited film increases its absorbance upon polypyrrole oxidation (Figure 8b) as expected for the overlapping of the gold SP band with the broad response of oxidized polypyrrole. It is in any case noteworthy that this occurs in the energy regions external to the SP band peak, where the absorbance remains almost unchanged. This appears to be an unusual feature linked to the combination of a conducting polymer shell over a gold nanoparticle surface.

The literature provides a satisfactory explanation for this result. In the steady-state absorption spectra of gold–polypyrrole nanoparticles with 25 nm diameter,[44] the SP band exhibits a 50% absorbance decrease in comparison with that of the bare gold nanoparticles.[44] The changes in the steady-state absorption spectrum are due to the difference in the dielectric constant of the surrounding medium and embedding material. In our case a decrease of the maximum absorbance and band broadening, attributable to a difference in the dielectric constant of the oxidized (conducting) and neutral (insulating) polymer layer is responsible for the absorbance dip at 550 nm and of the coupled satellite maxima at ca. 440 and 650 nm.

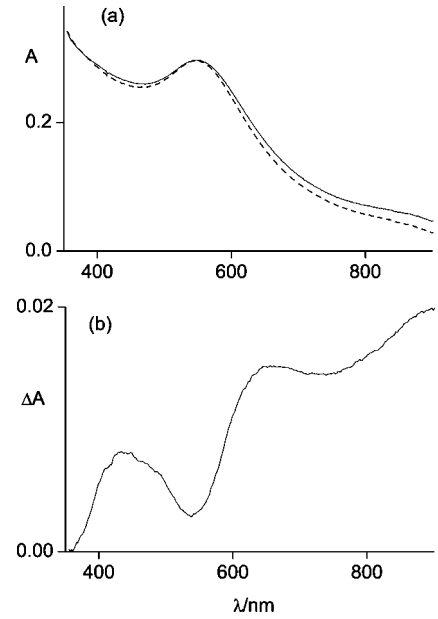

Figure 8. In-situ UV–vis spectra (a) of poly(PY–Au) film on ITO (---) before and (—) after oxidation at 0.5 V. (b) Differential spectrum.

(44) Shin, H. J.; Hwang, I. W.; Hwang, Y. N.; Kim, D.; Han, S. H.; Lee, J. S.; Cho, G. *J. Phys. Chem. B* **2003**, *107*, 4699.

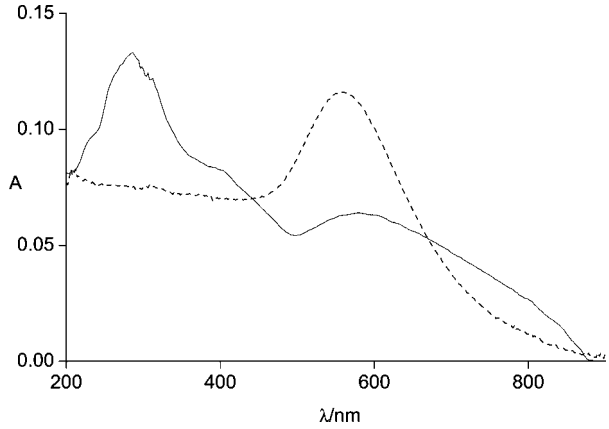

Figure 9. UV–vis spectra of PY-Au film on quartz (---) before and (—) after iodine coupling.

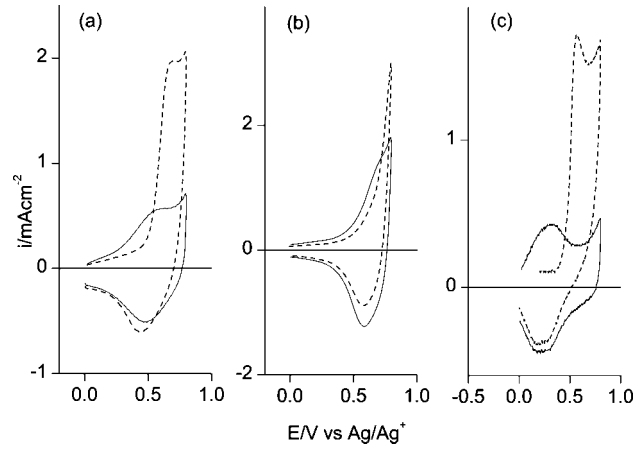

Figure 10. Cyclic voltammograms of (a) Me_2T_3–Au, (b) He_2T_3–Au, and (c) He_2CPDT–Au film in acetonitrile + 0.1 M Bu_4NClO_4 (---) first scan and (—) after potentiostatic oxidation. Scan rate: 0.1 V s^{-1}.

The intensity of the polypyrrole band is considerably lower than that of the SP band, as a consequence of the small amount of polymer compared to the gold mass. For this reason a minor change in the SP bandwidth has the observed major changes in the differential spectrum. The result, which shows clearly the influence of the conductive state of the polymer on the gold SP band, is also a patent demonstration of the different nature of the polymer sheet and of the gold core–electron structure, namely the localized and the collective character of the two modes of electronic absorption.

Iodine Coupling. The UV–vis spectrum of a PY–Au film on quartz (Figure 9) after iodine coupling records the broadening and red shift (from 560 to 580 nm) of the SP band and the appearance of a new band at 290 nm attributable to the α-coupled pyrrole moieties. In fact, the PY homopolymer displays its maximum at a longer wavelength (317 nm[19]), which appears to indicate a lower degree of polymerization and/or pyrrole ring decoplanarization in the AuNPs, as expected from the surface localization of the PY units on the gold clusters. From interpolation between the optical energy gap of the monomer and that of the polymer (DP = 13[19]), we may estimate a DP = 4 for the oligomeric chains linking the gold particles. This result is in substantial agreement with the electrochemical result (DP = 4) given above.

The FTIR spectrum of poly(PY–Au) shows that the original bands of the monomer are kept but for the disappearance of the strong band at 760 cm^{-1} due to CH out-of-plane bending of the 2 and 5 hydrogen atoms of the pyrrole rings, as expected from extensive α-coupling.

3.3.2. Oligothiophenethiol-Capped AuNPs. *Solid-State Electrochemical Coupling.* The Me_2T_3–Au film shows an irreversible oxidation process at the same potential of the monolayer on the gold electrode (Figure 10a). Upon repetitive cycling over the process the CV develops the redox response at $E^0 = 0.55$ V attributable to T6 moieties formed by anodic coupling.

At difference He_2T_3–Au films show their irreversible oxidation process as a slope shifted anodically to ca. 1 V (Figure 10b), but in spite of this unfavorable displacement repetitive cycling can develop the redox response at $E^0 = 0.65$ V due to T6 moieties.

The He_2CPDT–Au film is oxidized at 0.60 V (Figure 10c) where repetitive cycling develops the redox response at $E^0 = 0.30$ V attributable to oligomers formed by anodic coupling, as in the monolayer.

The reversible charge stored in the redox process of all organometallic polymers is 40–50% of the total irreversible oxidation charge. Moreover, the materials are insoluble in chloroform as expected.

Solution Electrochemical Coupling. Me_2T_3–Au dissolved in CH_2Cl_2 is irreversibly oxidized as the films and repetitive scans produce again the CV response of the formed polymer film. Differently from the methyl-substituted homologue, the cyclic voltammogram of He_2T_3–Au shows the irreversible oxidation as an ill-defined process anodically shifted to ca. 0.9 V, and repetitive scans do not produce any increase in the CV response. Also, He_2CPDT–Au dissolved in CH_2Cl_2/$CHCl_3$ shows the same irreversible oxidation shifted from 0.6 V (for the monolayer) to ca. 0.9 V and associated with failure of electropolymerization.

It appears that the difficult oxidation (slow electron transfer) of the oligothiophene moiety, attributable to strong solvation of the lipophilic alkyl substituents by the chlorinated solvent, may account for the failed electropolymerization.

From the whole electrochemical analysis of capped nanoparticles it may be concluded that for an efficient electrochemical coupling also in account of material saving solid state is in general preferable to solution processing.

Iodine Coupling. After iodine treatment the UV–vis spectrum of Me_2T_3–Au and He_2T_3–Au films on ITO (Figure 11) records the shift of the maxima at 400 and 590 nm to 440 and 660 nm, attributable to the coupled T6 moieties and to stronger SP interaction of the gold particles, respectively.

The FTIR spectra of the polymer films indicate the increase of a band at 830–840 cm^{-1} due to the aromatic C–H out-of-plane vibrations characteristic of 2,5-disubstituted-3-alkylthiophene[45] and in our case to the hydrogen atoms close to the dimerization site.

(45) Hotta, S.; Rughooputh, S. D. D. V.; Heeger, A. J.; Wudl, F. *Macromolecules* **1987**, *20*, 212.

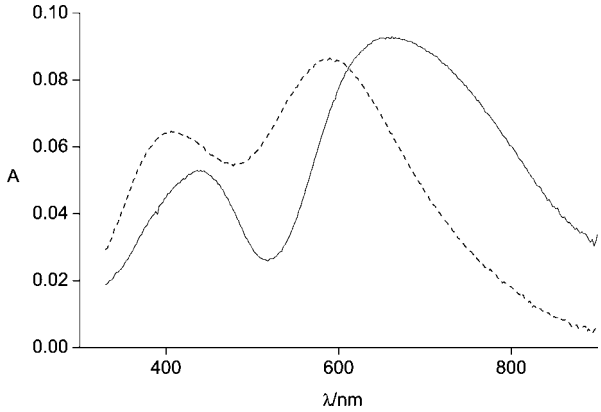

Figure 11. UV–vis spectra of He_2T_3–Au film on ITO (---) before and (—) after iodine coupling.

3.4. Conductivity of Thiol-Capped AuNPs. Films of clusters cast from chloroform solution on the microband array display an appreciable conductivity which is changed by iodine coupling to polymer clusters. Conductivity values for our structures before and after iodine coupling are summarized in Table 2.

R–Au Clusters. The conductivity of thiol-capped gold clusters has been particularly investigated in the past for alkyl[46] and alkylaryl thiols.[47] Here we consider our series of pyrrole- and thiophenethiol clusters comparing the results with those of some homologues in the literature.

PY–Au films display a conductivity of 3×10^{-7} S cm^{-1}. The value is comparable to that of analogous composites in general[48] but ca. 100 times lower than that (2×10^{-5} S cm^{-1}) of 3-thienylhexanethiol-capped AuNPs of comparable size (4.2 nm).[49] It is likely that the thiophene is better conducting then the *N*-alkylpyrrole since the latter ring is capped by alkyl substituents also at the 3- and 4-positions.

He_2T_3–Au films give a conductivity of 1×10^{-3} S cm^{-1}, i.e., much higher than for 3-thienylhexanethiol-capped AuNPs,[49] as a consequence of direct linkage of thiophene to gold and/or higher conjugation. For comparison, T_3PPh_2-capped 1.7-nm AuNPs have shown a conductivity of 5×10^{-5} S cm^{-1}.[14] The role of the gold nanoparticle size is evident in the higher conductivity of the 5 nm particles. The conductivity of Me_2T_3–Au is 5-fold lower than that of He_2T_3–Au, which may be due to better ordering in the latter promoted by the longer alkyl chains.

He_2CPDT–Au films have a conductivity of 1×10^{-2} S cm^{-1}, which is the highest value for the investigated AuNPs, in spite of the presence of the alkyl chain spacer and of the reduced conjugation. It is likely that a higher conduction along ordered bithiophene chains, disposed among the gold clusters, is responsible for this result. In fact, it was found that in polythiophene layers the orientation of the conjugated plane to the surface plane changes strongly the electron mobility.[50] Thousand times higher mobilities are observed when the polythiophene molecular planes are perpendicular, rather than parallel, to the surface plane. Thus a similar face-to-face orientation of the CPDT moieties may be present and favor charge transport also in our case. In line with this suggestion, a very recent paper[51] has evidenced the involvement of π-interactions in the conduction of phenylethylthiol-capped AuNPs.

Poly(R–Au) Clusters. After iodine coupling to polymer the conductivity of the films is increased in all cases. Unfortunately, iodine coupling of He_2CPDT–Au samples, which makes them insoluble as expected from cross-coupling, did not allow conductivity to be measured due to mechanical problems of the polymer.

The conductivity of PY–Au films is increased by 5 orders of magnitude, which is accounted for by enhanced transport via the polyconjugated polymer chains.

The conductivity of He_2T_3–Au and Me_2T_3–Au increase by 2 orders of magnitude, attaining ca. 1×10^{-1} S cm^{-1} in the former. For comparison, the conductivity of T_3PPh_2-capped 1.7 nm AuNPs increases from 5×10^{-5} to 3×10^{-2} S cm^{-1} upon (electrochemical) coupling.[14]

It is surprising that the conductivity values of the poly(R–Au) polymers, falling in the range 2×10^{-2}–1×10^{-1} S cm^{-1}, are comparable among them and in comparison with those of the polymeric clusters described below. This means the different pathways for conduction, namely the direct bridge (along the gold–gold direction) and the sideway bridge (tangent to the gold particle), do not give distinguished behaviors, as if a bottleneck for conduction is present in these structures.

3.5. Solvoconductivity of Thiol-Capped AuNPs. In recent times there has been a huge demand for sensors for volatile organic compounds with polymer array sensor based mainly on the conductivity change upon solvent swelling. In particular, gold colloids[52] have been investigated, and here we have done the same with π-conjugated linkers. Analogous measurements were performed previously with 3-thienylalkylthiol-capped gold nanoparticles.[49]

We have deposited He_2T_3–Au cluster films on the microband electrode from 1% chloroform solution. Then resistance measurements were performed alternately in air and under vapor pressures close to saturation. The observed conductivity changes, which are very reproducible, are given as ratio to the conductivity in air (Table 2). The responses are fast with typical response times of 0.2–0.5 s.

The conductivity of He_2T_3–Au clusters decreases (negative solvoconductivity) for all solvents (Figure 12), which is attributable to separation of the nanoparticles by the swelling

(46) Wuelfing, W. P.; Green, S. J.; Pietron, J. J.; Cliffel, D. E.; Murray, R. W. *J. Am. Chem. Soc.* **2000**, *122*, 11465.
(47) Wuelfing, W. P.; Murray, R. W. *J. Phys. Chem. B* **2002**, *106*, 3139.
(48) Bethell, D.; Brust, M.; Schiffrin, D. J.; Kiely, C. *J. Electroanal. Chem.* **1996**, *409*, 137.
(49) Ahn, H.; Chandekar, A.; Kang, B.; Sung, C.; Whitten, J. E. *Chem. Mater.* **2004**, *16*, 3274.
(50) Sirringhaus, H.; Brown, P. J.; Friend, R. H.; Nielsen, M. M.; Bechgaard, K.; Langeveld-Voss, B. M. W.; Spiering, A. J. H.; Janssen, R. A. J.; Meijer, E. W.; Herwig, P.; de Leeuw, D. M. *Nature (London)* **1999**, *401*, 685.
(51) Pradhan, S.; Ghosh, D.; Xu, L. P.; Chen, S. *J. Am. Chem. Soc.* **2007**, *129*, 10622.
(52) (a) Vohitjen, H.; Snow, A. W. *Anal. Chem.* **1998**, *70*, 2856. (b) Evans, S. D.; Johnson, S. R.; Cheng, Y. L.; Shen, T. *J. Mater. Chem.* **2000**, *10*, 183. (c) Franke, M. E.; Koplin, T. J.; Simon, U. *Small* **2006**, *2*, 36. (d) Wang, L.; Shi, X.; Kariuki, N. N.; Schadt, M.; Wang, G. R.; Rendeng, Q.; Choi, J.; Luo, J.; Lu, S.; Zhong, C. J. *J. Am. Chem. Soc.* **2007**, *129*, 2161.

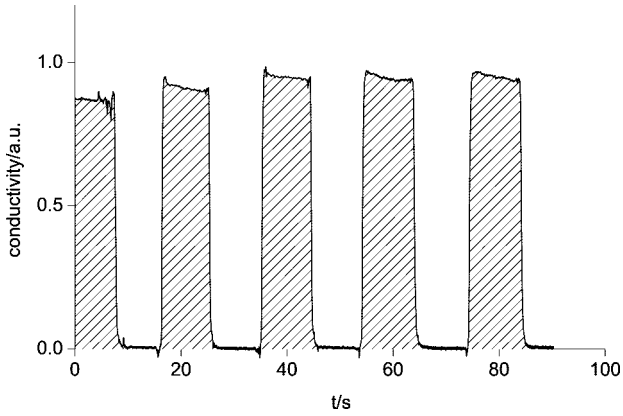

Figure 12. Conductive response of He_2T_3–Au film on microband array alternating air and chloroform-saturated air.

Table 3. Relative Conductivity Change ($\Delta\sigma/\sigma_0$) and QCM Solvent/Gold Molar Ratio (R) at Various Solvents[a,b] (Saturated Air) for He_2T_3–Au Clusters

	AN(36)	EtOH(24)	AC(22)	$CHCl_3$(4.9)	TOL(2.4)	HEX(1.9)
$\Delta\sigma/\sigma_0$	−0.24	−0.27	−0.60	−1	−1	−0.86
R	0.08	0.04	0.06	0.6	0.6	0.4

[a] Dielectric constant in parentheses. [b] AN = acetonitrile, AC = acetone, TOL = toluene, and HEX = *n*-hexane.

solvent. The order (see Table 3) is the same of the solubility, confirming previous findings.[49]

The solvent uptake by the polymer films was measured by QCM. The uptake was in any case reversible since nitrogen fluxing restored the starting weight completely. The values of the solvent/gold molar ratio (Table 3), which are correlated to the solubility of the cluster, follow the solvoconductivity trend.

In metal nanoparticle aggregates charges move from gold to gold according to a hopping mechanism, i.e., via tunneling through the intervening monolayer structures.[53,54] Alternatively, a percolation model has been proposed for this type of conduction.[55] The solvent molecules enter the cluster matrix, increasing the distance between the hopping sites.

For the iodine-coupled polymers we have considered, namely poly(He_2T_3–Au) and poly(PY–Au), in which the deposit is made insoluble by cross-linking, QCM shows that chloroform is still heavily incorporated, with a $CHCl_3$/Au molar ratio $R = 0.4$ and 0.6, respectively, close to that for the non-cross-linked clusters. For these polymer materials the conductivity still decreases reversibly with exposure to chloroform, but changes are minor. Moreover, films must be thin enough (1 μm or less) both to allow fast solvent exchange and to resist mechanical strain, since mechanical failure easily occurs. Thus, it appears that cross-linking, which stabilizes the films vs dissolution, is not favorable to promote solvoconductive responses.

3.6. Polythiophenethiol-, Oligothiophenedithiol-, and Ethanedithiol-Capped Gold Surfaces. These cases are distinguished from those of the monothiols described above since capping of AuNPs may occur at multiple sites of the ligand, thus causing cross-linked polymer formation. In fact, mixing AuNPs and any of the polythiols above in solution causes the formation of insoluble polymer structures.

Also, self-assembled monolayers of α,ω-dithiols may show both parallel and upright surface orientation[56] and multilayer formation. Therefore, the layers (with the exception of PATSH and EDT, see below) have been more safely deposited from the acetyl-protected dithiol.[16]

The PATSH monolayers were assembled from 10^{-4} M solution. In fact, deposition from a 10-fold more concentrated solution gives the same identical results, so that cross-linking through disulfide formation is ruled out. In any case operating with a more dilute solution presents less risk of aggregation and polymerization in solution.

EDT is the shortest dithiol used for AuNPs multilayer formation. EDT layers are formed differently depending on the solvent and concentration.[31] Intermolecular disulfide bond forms and even tetralayers are assembled from hexane while mono/bilayers are formed in alcohols. We have therefore adopted the same direct method for our layering procedure using the dithiol in ethanol.

In the following section we describe monolayer formation on a gold surface summarizing the obtained electrochemical and optical parameters in Table 1. In a further section we report the subsequent formation of multilayers by sequential (LBL) adsorption of AuNPs and polythiol or dithiol, as illustrated in Scheme 2d and summarizing the electrochemical, optical, and conductivity parameters in Table 2. The resulting polymer structures are then compared with those produced by coupling of the thiol-capped AuNPs described above.

3.6.1. SAMs of PATSH on Gold. The PATSH monolayer on gold is reversibly oxidized in a single process at $E^0 = 0.57$ V (Figure 13a). The oxidation charge involved in this CV cycle at 0.9 V is 50 μC cm^{-2}. In P3OT ca. 0.3 electrons per thiophene ring are exchanged[57] so that the coverage degree (in thiophene subunits) may be evaluated from the redox charge as ca. 17×10^{-10} mol cm^{-2}. This value is impressively high compared with those of the monomeric linkers ($(2–4) \times 10^{-10}$ mol cm^{-2}, see Table 1), which indicates that the rigid-rod chains are not flat linked to the surface. In contrast with the anodic response, no significant charge is measured in cathodic stripping, which indicates a scarce number of gold sulfide linkages. These data together indicate that the polythiol coordinates the gold surface through a very limited amount of ends, with the rigid-rod oligothiophene chains floating out of the gold surface in a fluffy thiophene-rich layer.

Differently from the monolayer, the CV of a PATSH bulk film (Figure 13b) shows a twin reversible oxidation process at a lower potential ($E^0 = 0.15$ and 0.55 V), i.e., the same electrochemical characteristics displayed by P3OT.[58] This

(53) Zamborini, F. P.; Leopold, M. C.; Hicks, J. F.; Kulesza, P. J.; Malik, M. A.; Murray, R. W. *J. Am. Chem. Soc.* **2002**, *124*, 8958.
(54) Wang, G. R.; Wang, L.; Rendeng, Q.; Wang, J.; Luo, J.; Zhong, C. J. *J. Mater. Chem.* **2007**, *17*, 457.
(55) (a) Muller, K. H.; Hermann, J.; Raguse, B.; Baxter, G.; Reda, T. *Phys. Rev. B* **2002**, *66*, 754171. (b) Muller, K. H.; Wei, G.; Raguse, B.; Myers, J. *Phys. Rev. B* **2003**, *68*, 1554071.
(56) Leung, T. Y. B.; Gerstenberg, M. C.; Lavrich, D. J.; Scoles, G.; Schreiber, F.; Poirier, G. E. *Langmuir* **2000**, *16*, 549 and references therein.
(57) Zotti, G.; Zecchin, S.; Schiavon, G.; Vercelli, B.; Berlin, A.; Dalcanale, E.; Groenendaal, L. *Chem. Mater.* **2003**, *15*, 4642.
(58) McCullough, R. D.; Tristam-Nagle, S.; Williams, S. P.; Lowe, R. D.; Jayaraman, M. *J. Am. Chem. Soc.* **1993**, *115*, 4910.

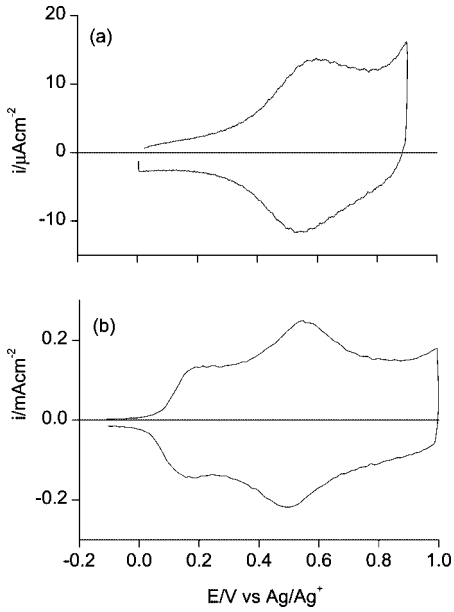

Figure 13. Cyclic voltammograms of (a) PATSH monolayer on gold and (b) PATSH film in acetonitrile + 0.1 M Bu_4NClO_4. Scan rate: 0.1 V s^{-1}.

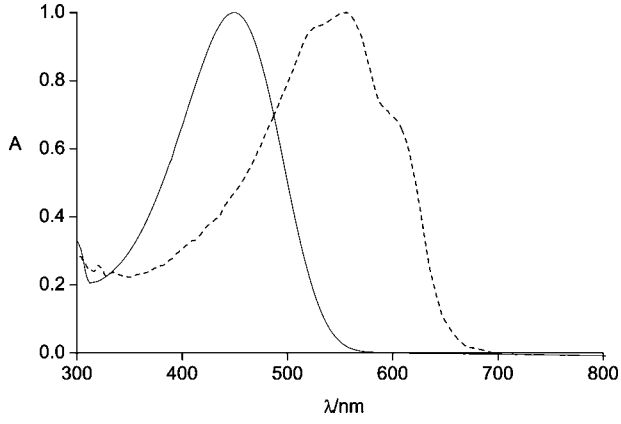

Figure 14. UV–vis spectra of PATSH (—) in chloroform and (---) as film on ITO.

result confirms the regioregularity of the polymer in the solid state whereas the positive shift in the monolayer redox potential and the single (not split) CV response suggests that the layer is characterized by a surface-induced disorder, in line with the indications given above.

The PATSH monolayer on AuNPs-primed ITO/glass shows, besides the SP band at 560 nm, the polythiophene absorption at 470 nm. A bulk PATSH film on ITO shows a maximum at 555 nm, with additional shoulders at 525 and 610 nm (Figure 14), i.e., with vibronic features characteristic of a regular and rigid backbone structure.[59] In chloroform solution the band is not structured, and its maximum is observed at a lower wavelength (450 nm, Figure 14), i.e., with a strong hypsochromic shift attributable to decoplanarization of the thiophene rings by solvation of the side substituents (solvatochromism). The same optical characteristics are displayed by P3OT. These last results are comparable with those observed for the PATSH monolayer and suggest that the adsorbed PATSH chains are similarly disordered, in agreement with the electrochemical analysis given above.

It is noteworthy that parallel changes in photoemission have been observed in P3OT films where gold nanoparticles had been introduced,[60] causing an analogous deviation from coplanarity (i.e., disorder) in correspondence of the gold centers.

The PATSH absorbance at 470 nm is ca. 20×10^{-3} au for both sides of the ITO/glass electrode, which value coupled with the extinction coefficient in chloroform solution (7×10^3 M^{-1} cm^{-1}, concentration expressed in thiophene subunits) allows to evaluate a coverage degree of ca. 14×10^{-10} mol cm^{-2}, in very good agreement with the CV coulometric result.

3.6.2. SAMs of $He_4T_6(SAc)_2$ and $T_3(SAc)_2$ on Gold. The $He_4T_6(SAc)_2$ monolayer on gold is reversibly oxidized with 80 μC cm^{-2}. This value is very reproducible which rules out the occurrence of S–S polymerization of the ligand. On the basis of the two-electron reversible oxidation of a sexithiophene moiety, the coverage degree may be evaluated as 4×10^{-10} mol cm^{-2}. A sharp reduction peak in cathodic stripping involves a charge of 40 μC cm^{-2}. Given the one-electron characteristics of this reduction process, the fact that this value is right half the oxidation charge confirms that oligomeric species from S–S coupling are not present on the surface.

The $T_3(SAc)_2$ monolayer on gold undergoes reduction with an overall charge of 60 μC cm^{-2}. It must be remembered that the carbonyl end of the layer is not reduced in the used potential region down to −1.4 V. On the basis of the one-electron reduction of gold sulfide, the coverage degree may be evaluated as 6×10^{-10} mol cm^{-2}, which is considerably higher than that of other oligothiophenes. This appears to be due to the side packing ability of the T_3 moiety free from alkyl substituents.

The $He_4T_6(SAc)_2$ monolayer on AuNPs-primed ITO/glass shows the SP band at 570 nm and an additional absorption due to the sexithiophene moiety at 445 nm (vs 420 nm of $He_4T_6(SAc)_2$ in chloroform solution). Similarly, the $T_3(SAc)_2$ monolayer shows the SP band at 560 nm and the T3 band shifted from 375 nm in solution to 425 nm.

3.6.3. SAMs of EDT on Gold. The EDT monolayer on gold undergoes its irreversible cathodic stripping in a sharp peak where the passed charge, which is the same on samples prepared with 1 or 18 h of exposure, is very high (180 μC cm^{-2}) if we recall that alkyl thiols display charges up to 100 μC cm^{-2}.[61] At the same time the capacitive current of gold is strongly depressed, which indicates that the films are very compact. The high charge may be attributed to the presence of S–S bonds, which undergo a two-electron reduction process.[62] Therefore, a bilayer would be reduced

(59) (a) Chen, T. A.; Wu, X.; Rieke, R. D. *J. Am. Chem. Soc.* **1995**, *117*, 233. (b) Tachibana, H.; Hosaka, N.; Tokura, Y. *Macromolecules* **2001**, *34*, 1823.

(60) Sarathy, V. K.; Narayan, K. S.; Kim, J.; White, J. O. *Chem. Phys. Lett.* **2000**, *318*, 543.

(61) Kakiuchi, T.; Usui, H.; Hobara, D.; Yamamoto, M. *Langmuir* **2002**, *18*, 5231.

(62) Stricks, W.; Frishmann, J. K.; Mueller, R. G. *J. Electrochem. Soc.* **1962**, *109*, 518.

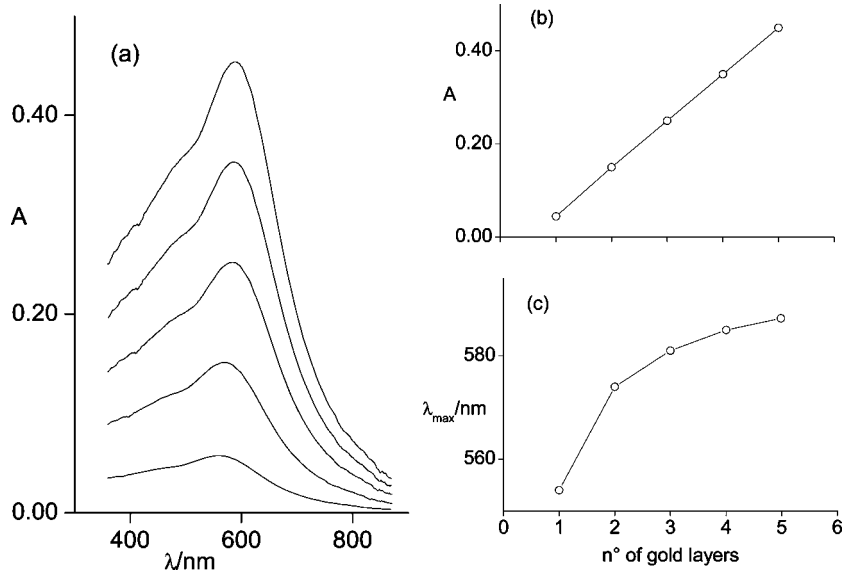

Figure 15. UV–vis (a) spectra and relevant (b) maximum SP absorbance and (c) maximum wavelength of $(Au/PAT)_n$ multilayer growth on ITO/MTS/Au.

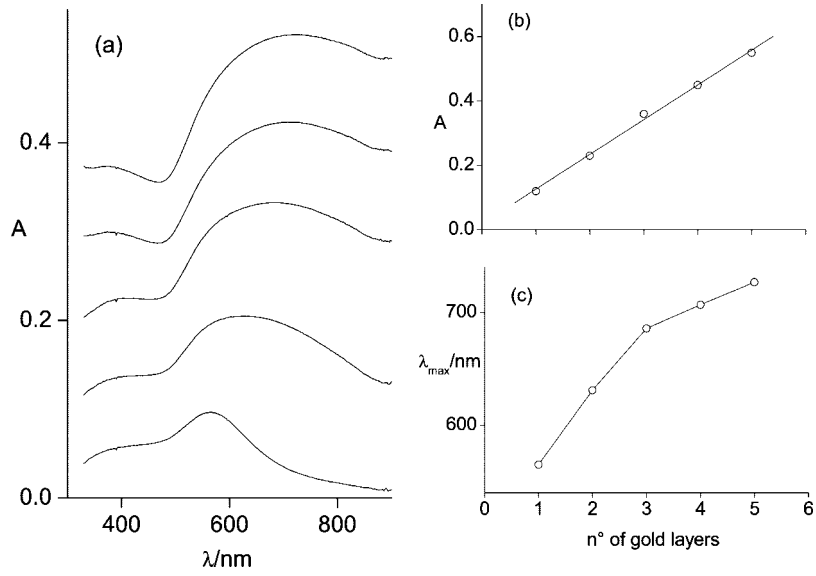

Figure 16. UV–vis (a) spectra and relevant (b) maximum SP absorbance and (c) maximum wavelength of $(Au/EDT)_n$ multilayer growth ($n = 1$–5) on ITO/MTS/Au.

in an overall three-electron process vs one electron for a monolayer so that our layer results to be intermediate between a monolayer and a bilayer, in full agreement with the literature results.[31]

3.7. Polythiophenethiol-, Oligothiophenedithiol-, and Ethanedithiol–Gold Multilayers. The multilayer structures ITO/MTS/$(Au/R)_n$ ($n = 1$–5) have been progressively formed LBL, i.e., by dipping for 1 h the gold-primed ITO alternatively in $R(SAc)_2$ or PATSH and AuNPs solutions, as illustrated in Scheme 2d.

The SP optical growth of $(Au/R)_n$ ($n = 1$–5, Figures 15 and 16) is linear with n with a slope of 0.1 au layer^{-1}. The reversible charge in the oxidative CV of the $(Au/PAT)_n$ multilayer corresponds to an average of 70 μC cm^{-2} layer^{-1} for the polymer layers beyond the first one (storing 50 μC cm^{-2}). Similarly in $(Au/He_4T_6)_n$ the stored reversible charge increases from 80 μC cm^{-2} layer^{-1} for the first layer to 110 μC cm^{-2} layer^{-1} for the subsequent layers, whereas on the contrary in $(Au/T_3)_n$ the oligothiophene irreversible oxidation charge (90 μC cm^{-2} layer^{-1}) is the same as the monolayer. Thus, it appears that for the longer thiophene oligomers and polythiophene subsequent layers grow at a rate faster than the amount of the starting monolayer, possibly as a consequence of the increased roughness introduced by gold nanoparticles.

Spectroscopy and AFM. The spectrum of the $(Au/He_4T_6)_5$ multilayer evidences the shift of the SP band from 570 nm in the monolayer to 610 nm, as previously observed for multilayers of AuNPs and terthiophene.[63] Passing to the $(Au/T_3)_5$ structure, maxima are displayed at 440 and 640 nm, i.e., with the strongest red shift of both the oligothiophene and the SP bands. This indicates an even stronger interaction

(63) Vercelli, B.; Zotti, G.; Berlin, A. *Chem. Mater.* **2007**, *19*, 443.

between the gold and terthiophene moieties via the short conjugated bridge. Finally, the spectra of the $(Au/EDT)_n$ structures ($n = 1$–5) display broad SP maxima shifting progressively with increasing n from 650 to 750 nm (Figure 16), i.e., with the strongest observed red shift of the SP band. A very strong interaction between the gold particles via the short S–C–C–S bridge is therefore evidenced.

AFM imaging of the $(Au/PAT)_{10}$ and $(Au/He_4T_6)_5$ multilayers displays uniform surfaces with a roughness of 6 and 4 nm and domains ca. 25 and 150 nm wide, respectively.

All the multilayers are strongly bound to the substrate since they stand the scotch tape strip test without any loss of material.

Conductivity. The $(Au/PAT)_{10}$, $(Au/He_4T_6)_5$, and $(Au/T_3)_5$ multilayers display surface resistivities of ca. 5×10^6 Ω sq^{-1}. From the thicknesses of 90, 30, and 15 nm, respectively, the bulk conductivities, given in Table 2, range from 2×10^{-2} to 1×10^{-1} S cm^{-1}.

The conductivity of the T3-based structure is twice that of the T6-based structure, as expected from the shorter bridge. We must recall that the $(Au/T_3)_n$ structure was previously studied on interdigitated gold electrodes,[23] where a higher conductivity (3.0 S cm^{-1}) was measured. The procedure for the structure buildup was in any case not comparable with the LBL one we adopted in this work.

The conductivity and color of the $(Au/PAT)_{10}$ layers does not change appreciably after a 3 day exposure to iodine vapors, which indicates scarce or null I_2 doping. Also, 2 h heating at 120 °C does not alter the conductivity, which suggests that no coalescence of the gold particles occurs. Both results are compatible with a rigid and extended cross-linking.

In the case of $(Au/He_4T_6)_5$, differently from the $(Au/PAT)_n$ multilayers above, heating for 2 h at 120 °C increases the conductivity by 2–3 times. It appears that the extended cross-linking is modified according to a rearrangement of the sexithiophene linkers. An analogous decrease in the resistance of colloidal gold multilayer films upon heating was observed when the linker molecules were 1,6-alkanedithiols[64] and was attributed to coalescence of the gold particles to form more conducting pathways.

The $(Au/EDT)_5$ multilayer attains 2×10^5 Ω sq^{-1}, and from a thickness of 20 nm a bulk conductivity of 2.5 S cm^{-1} is evaluated with an impressive 25-fold increase compared with the T3 structure. It must be mentioned that a 16-multilayer of this type has been recently assembled from toluene and 8 nm gold nanoparticles.[65]

3.8. Conductivity of Conjugatively Interlinked AuNPs. An ensemble of conjugatively interlinked AuNPs may be considered as an organometallic polymer constituted by a gold cluster and the –AuS–B–SAu– architecture as repeat units. In such structures each sulfur-linked gold atom is part of a gold nanoparticle, where electron transport is metallic and therefore fast, and B is the polyconjugated bridge. Electron transport across –AuS–B–SAu– depends strongly on the position of the Fermi level of the metal relative to the lowest unoccupied molecular orbital (LUMO) and the highest occupied molecular orbital (HOMO) of the molecular bridge including the sulfur atoms.[66] If the Fermi level approaches the energy of the molecular orbitals of the molecular bridge, resonant electron transfer may take place, and the conduction of electron will occur through the molecular orbitals (MOs), which are affected by interaction with the contacts.

A MO favorable for conduction requires it to be delocalized while connecting the molecule to the contact electrodes at both ends. The molecule is in a conducting state if delocalized orbitals are available in the energy range for which one contact has occupied levels and the other has unoccupied ones. The molecule is in a nonconducting state if those orbitals are localized; i.e., both ends of the molecule behave as an insulating layer to the contacts even when the molecular backbone itself is delocalized.

The Au–S interface provides a particularly poor characteristic, which can be considered "insulating" for electron transport. Hence, the –AuS–B–SAu– architecture can be considered as consisting of a central quantum well (characterized by discrete electronic levels) separated from two metallic leads by two thin "insulating" barriers. Under such conditions, there is no connection of the LUMO of the molecule with the two terminals.

Considering now the results of our investigation, we observed that the conductivity values of the polymeric clusters fall in the narrow range 2×10^{-2}–1×10^{-1} S cm^{-1} (see Table 2). Also, a simple tetrathiol–AuNPs structure such as the MP4–Au multilayer (MP4 is tetrathiol pentaerythritol tetrakis(3-mercaptopropionate; see Chart 1), with a conductivity of 5×10^{-2} S cm^{-1},[63] is well comprised in this range. Moreover, looking in the literature, we find that T_3PPh_2-capped 1.7 nm AuNPs in the poly(T3-Au) structure show a maximum conductivity of 8×10^{-2} S cm^{-1}.[14] A series of dithiol-AuNPs (5 nm Au) LBL films display the same maximum conductivity of 8×10^{-2} S cm^{-1},[48] and in a series of monodisperse (2 and 4 nm gold) dithiol-AuNPs with linear alkane spacers the maximum conductivity is 10^{-1} S cm^{-1}.[54]

After all these results a limiting value of 10^{-1} S cm^{-1} for the conductivity appears to be operating in all dithiol-linked gold clusters.

Two facts are against this suggestion, namely a previous report and a result of ours here reported. Very recently, network structures made of oligothiophene dithiols and gold nanoparticles were formed by mixing the components on interdigitated gold electrodes,[23] and in the case of terthiophene the conductivity of the structure was found to be 30-fold higher (3.0 S cm^{-1}) than that we have prepared via LBL. In any case we believe that the methods for such structure preparation are too much different to allow a significant comparison to be made.

The other fact is that the EDT multilayer structure we have prepared for comparison displays a conductivity which is

(64) Supriya, L.; Claus, R. O. *Chem. Mater.* **2005**, *17*, 4325.
(65) Fishelson, N.; Shkrob, I.; Lev, O.; Gun, J.; Modestov, A. D. *Langmuir* **2001**, *17*, 403.
(66) (a) Fan, F. R.; Yang, J.; Cai, L.; Price, D. W.; Dirk, S. M.; Kosynkin, D. V.; Yao, Y.; Rawlett, A. M.; Tour, J. M.; Bard, A. J. *J. Am. Chem. Soc.* **2002**, *124*, 5550. (b) Fan, F. R.; Lai, R. Y.; Cornil, J.; Karzazi, Y.; Brédas, J. L.; Cai, L.; Cheng, L.; Yao, Y.; Price, D. W.; Dirk, S. M.; Tour, J. M.; Bard, A. J. *J. Am. Chem. Soc.* **2004**, *126*, 2568.

similarly well above the supposed limiting conductivity. Yet in an EDT/AuNPs 16-multilayer recently assembled via LBL from toluene,[65] the analysis of the temperature dependence of conductivity has shown that in such a material contacts direct and via ligand are mixed, making impossible the evaluation of each contribution and therefore overestimating the interparticle conductivity.[65] Apparently, charge transport levels off when the conductivity of the molecular bridges is high so that the limit should be attributed either to the nature of the gold nanoparticle itself or to its Au–S handles.

According to the first possibility, we must stress that arrays of nanocrystal gold molecules behave as weakly coupled molecular solids comprising discrete nanoscale metallic islands separated by insulating ligand barriers.[67] The key parameters which are found to dominate charge transport are not only the internanocrystal tunnel barrier resistance, arising from the insulating ligands that separate the metal cores, but also the nanocrystal charging energy, governed by core diameter, dielectric properties of the ligand, and electrostatic coupling between neighboring cores. Similarly, gold nanoparticles with an average diameter of 4 nm have been found to work as Coulomb islands in the networked structure.[23] Anyway, the activation energies measured for such systems are some millielectronvolts only so that the possibility that this is the energetic limit to the conductivity found in our systems may be disregarded.

Considering the second hypothesis, it has been recently reported that in the single-molecule conductance of gold contacts bridged by alkanes terminated with dicarboxylic acid, diamine, and dithiol anchoring groups the prefactor of the exponential function, a measure of contact resistance, is highly sensitive to the type of the anchoring group and varies in the order of Au–S > Au–NH_2 > Au–COOH.[68] This large dependence is attributed to different electronic coupling efficiencies provided by the different anchoring groups between the alkane and the electrodes. These results suggests that more conductive responses may be obtained with other less strongly bound linkages than thiols.

In any case it is still possible that the limit of conductivity above is essentially a practical one, in the sense that decreasing the spacer length below certain values causes the appearance of direct contacts, thus making further analysis virtually impossible.

4. Conclusions

Novel pyrrolethiol- and thiophenethiol-capped gold nanoparticles have been produced and subsequently linked through electrochemical and chemical coupling. To this end, a series of new alkyl-substituted pyrrole- and thiophene-based thiols have been synthesized. The compounds, which form dense self-assembled monolayers on gold electrodes, react with gold nanoparticles to form monodisperse, stable, and soluble thiol-capped gold clusters with the same gold core diameter. These are electrochemically and chemically coupled to polymeric gold clusters linked by polyconjugated bridges. Analogous polymeric clusters have been prepared on gold-modified surfaces via alternation of gold nanoparticles and oligothiophene-based dithiols or a polythiophene polythiol.

The thiol-capped gold clusters give solvoconductive responses fast and stable, which parallel the degree of swelling by volatile organic solvents. Their conductivity, in the range $10^{-7}-10^{-2}$ S cm^{-1}, increases in all cases up to a narrow range of $2 \times 10^{-2}-10^{-1}$ S cm^{-1} when the polyconjugated ends of the gold clusters are connected to form polyconjugated bridges. Comparison with the literature appears to indicate 10^{-1} S cm^{-1} as a practical limit to the conductivity in such systems, possibly controlled by the Au–S junctions.

The new nanoparticles, where the gold particles are the same size and bear different conjugated ends or bridges, are expected to open interesting perspectives in the fields of modified electrodes for electrocatalysis and electroanalysis and of organic electronics.

Acknowledgment. The authors thank dr. G. Schiavon and dr. S. Zecchin of the CNR for helpful discussions and dr. M. Natali and S. Sitran of the CNR for their technical assistance.

CM071701Z

(67) Quinn, A. J.; Biancardo, M.; Floyd, L.; Belloni, M.; Ashton, P. R.; Preece, J. A.; Bignozzi, C. A.; Redmond, G. *J. Mater. Chem.* **2005**, *15*, 4403.
(68) Chen, F.; Li, X.; Hihath, J.; Huang, Z.; Tao, N. *J. Am. Chem. Soc.* **2006**, *128*, 15874.